Progress in Additive Manufacturing
https://doi.org/10.1007/s40964-026-01846-x

REVIEW

Invar alloys in advanced manufacturing: thermal treatment processes, properties, and applications

Fatih Altun[1] · Abdulhammed Hamzat[1] · Gozde Altuntas[2] · Abdulcelil Bayar[1] · Ramazan Asmatulu[1] · Eylem Asmatulu[1]

Received: 8 January 2026 / Accepted: 6 July 2026
© The Author(s) 2026

Abstract

This study will examine how Invar (an alloy of 36% nickel and 64% iron) works in advanced manufacturing, especially with the use of Additive Manufacturing Technologies such as Laser Powder Bed Fusion (LPBF) and Directed Energy Deposition (DED). The extremely low coefficient of thermal expansion (CTE) of Invar is the most widely recognized feature; nonetheless, this article, through a comprehensive and in-depth study, examines the AM-related microstructural elements such as porosity, phase distribution, and texture anisotropy that influence the thermal and mechanical properties of Invar. In addition, the paper goes on to explore the potential benefits of post-processing interventions, e.g., heating and cryogenic treatments, in residual stress relief, microstructure refining, and stabilization of functional properties. Process, structure, and property correlations across various additive manufacturing (AM) processes have rarely been integrated, resulting in a lack of thermal stability guidelines that simultaneously preserve mechanical integrity. In addition to the fluctuations in CTE measurement along with anisotropy and defect issues, it seems that processing and characterization methods have to be standardized. This review, by making the most out of present-day studies, aims to address these concerns and also compares conventionally and additively produced Invar alloys. As a result, the principal findings indicate that although residual stress, porosity, and microstructural heterogeneity are contributing factors to the emergence of new problems, suitable AM parameters can facilitate the rise in near full density and CTE values close to those of wrought materials. Besides, post-processing has a considerable influence on the continuation of dimensional stability and mechanical performance, yet the actual changes brought about geographically are still largely determined by the original process. Finally, this paper makes a contribution in suggesting future directions of work with regard to the ways and methods that will be necessary to accomplish the Invar alloy usage in such technologically advanced fields that will demand the highest level of the precision of the materials.

✉ Eylem Asmatulu
e.asmatulu@wichita.edu

Fatih Altun
fxaltun@shockers.wichita.edu

Abdulhammed Hamzat
akhamzat@shockers.wichita.edu

Gozde Altuntas
gozdealtuntas@gazi.edu.tr

Abdulcelil Bayar
celilbayar@gmail.com

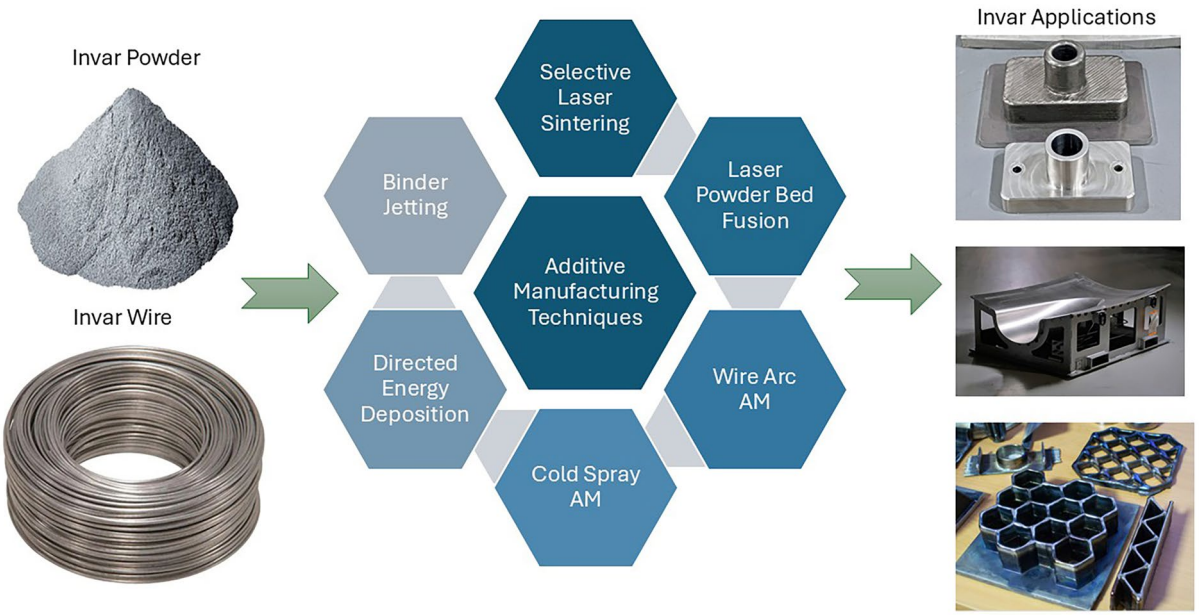
Ramazan Asmatulu
ramazan.asmatulu@wichita.edu

[1] Wichita State University, 1845 Fairmount St., Wichita, USA

[2] Gazi University, Ankara, Turkey

Published online: 03 August 2026

Graphical abstract



Keywords Invar alloys (Fe–Ni) · Additive manufacturing · Thermal expansion · Heat and cryogenic treatment · Applications

1 Introduction

Global interest in Invar alloys ($Fe_{64}Ni_{36}$) is increasing due to its widespread use in various industrial sectors, driven by its low thermal expansion below the Curie temperature (230 °C) and exceptional mechanical properties at cryogenic temperatures. Because of their low CTE (1.2×10^{-6}/°C), dimensional stability and cryogenic performances, these materials are used in oil and gas transportation, light bulbs and electronic vacuum systems, pendulum clocks, high-voltage transmission, aerospace, cryogenic storge container, thermostats, and electronic devices [1, 2]. Since its discovery by renowned British physicist Charles-Edouard Guillaume, who was awarded the Nobel Prize in Physics in 1920 for his invention, Invar exhibits very high ductility, which greatly affects its malleability. Invar alloy components often feature complex geometrical structures, including eggshell molds, porous structures, and satellite supports, among others. Typical applications of this alloy are illustrated in Fig. 1. Conventional manufacturing methods, such as welding, forging, and casting, involve high energy consumption, material wastage, longer processing times, challenges in producing complex geometries, and low molding efficiency [3–5]. Additionally, Invar alloys are susceptible to cracking during solidification, leading to work hardening that reduces the service life of the parts. Therefore, AM techniques like LPBF enable the production of complex internal structures with shorter production cycles and are considered suitable methods for preserving thermal expansion properties [6, 7].

The AM, also known as 3D printing, is a novel manufacturing process that uses three-dimensional models generated from a computer to fabricate complex components layer by layer. LPBF is a common metal AM process widely used to produce metal materials due to its advantages in design flexibility, high mold efficiency, and extensive design freedom. It is noteworthy that Invar has an austenitic structure and is very hard to machine, but it possesses good weldability properties [9, 10]. Extensive studies have investigated the properties of Invar components fabricated via AM techniques, particularly LPBF and Laser Melting Deposition (LMD) with a primary focus on the CTE and Curie temperature of the resulting materials [11–13]. For instance, Qui et al. [14] employed LPBF techniques to fabricate Invar 36 samples and examined the change in microstructures and other properties with respect to the process parameter. They observed that the as-built sample exhibits very low porosity at scanning speeds below 3200 mm/s, but the porosity increases significantly above 3200 mm/s. This can be attributed to increasing unstable melting flow behavior with irregular-shaped laser scanned tracks. Similarly, LPBF-fabricated Invar using island scanning techniques exhibits a dominant FCC γ phase, along with some sparse BCC α precipitates [15]. The microstructure of the manufactured material was characterized by fine columnar grains, with porosity being

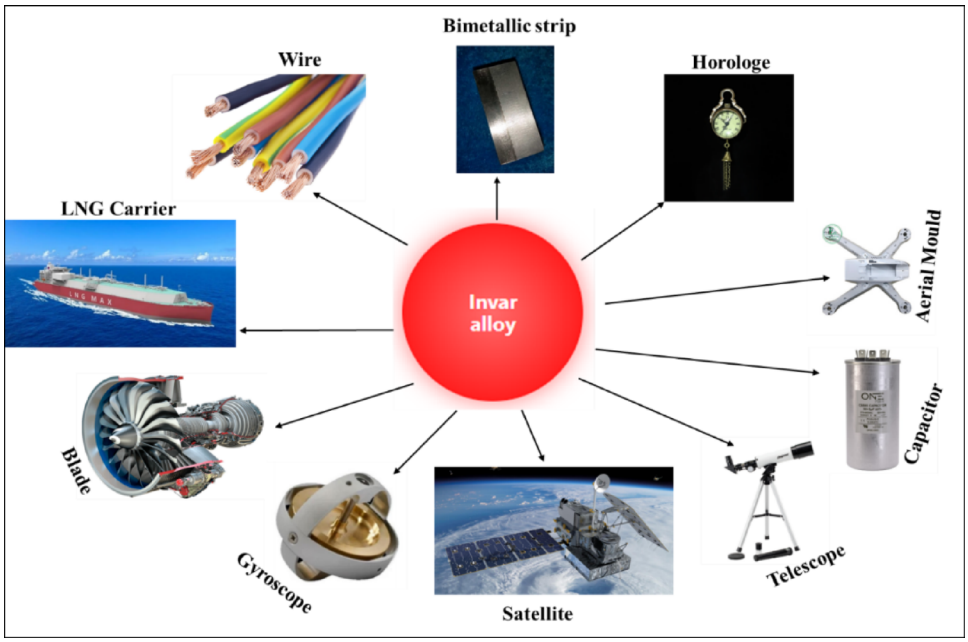


Fig. 1 Various industrial applications of Invar alloys [8]

highly dependent on laser energy density. Low energy densities caused significant lack-of-fusion porosity (up to 15%), whereas optimal densities (99.2–198.4 J/mm3) achieved near-fully dense parts (<0.4% porosity). The CTE was consistently lower than the wrought value, ranging from 1.72 to 1.96×10^{-6} °C^{-}1. This reduction was driven by two mechanisms: at low energies, high porosity accommodated thermal expansion, while at high energies, the evaporative loss of nickel became the dominant factor in reducing the CTE.

Asgari et al. used X-ray computed tomography (CT) to examine the microstructure, and structural integrity of Invar 36 alloy samples fabricated with LPBF technology [9]. At the higher laser powers, the level of porosity reduces significantly. Also, the samples show a density higher than 99.8% in all scenarios considered. The CTE was found to be indirectly proportional to relative density; its values were comparable to those of conventional Invar. Notably, the adopted process induced thermal expansion anisotropy that is dependent on the build orientation. Other important studies that interrogate the influence of process parameters [16–19] revealed a strong correlation with the produced part's hardness and tensile strength. The increment in building size clearly results in higher hardness, more porosity, lower elongation, and higher tensile strength of super Invar alloy fabricated using LPBF. Prior reviews have typically focused on either the thermal expansion behavior or the additive manufacturing of Invar alloys. By contrast, this review not only covers different additive manufacturing routes but also post-processing methods, e.g., heat and cryogenic treatments, and correlates these with application-specific thermal and mechanical performance requirements, thereby developing a comprehensive process-structure–property framework.

2 Literature review methodology

A structured literature search was first performed to find peer-reviewed studies on Invar alloys, especially focusing on additive manufacturing, heat treatment, cryogenic treatment, microstructure, properties, and applications. The main databases searched were Scopus, Web of Science, ScienceDirect, SpringerLink, and Google Scholar. The search mainly concentrated on papers published between 2010 and 2025, however, a few earlier groundwork papers have been included where necessary to explain the Invar effect, alloy composition, and historically established properties.

The search was done using various keyword combinations such as "Invar alloy," "Invar 36," "Fe, Ni alloy," "additive manufacturing," "laser powder bed fusion," "LPBF," "directed energy deposition," "DED," "wire arc additive manufacturing," "WAAM," "cold spray," "heat treatment," "annealing," "aging," "cryogenic treatment," "thermal expansion," "coefficient of thermal expansion," "microstructure," "mechanical properties," and "applications." Boolean operators such as AND and OR aided in refining the results. Initially, the screening was done on the basis of title, abstract, and keywords, and at the next stage, the full text of the most relevant papers was checked.

Only peer-reviewed journal articles or conference papers reporting experimental results, modeling, characterization, or application-related findings directly connected to Invar alloys were included. Particular attention was given to

studies dealing with process, structure, property relationships, especially of additively manufactured Invar materials because these topics form the central focus of this review. Non-peer-reviewed sources, unrelated to Invar-based alloys, lack of technical details, duplicate publications, marginal coverage of topics in this review were excluded.

Following the screening stage, the core studies have been identified mainly by their relevance, technical depth, importance by citations, and their direct contributions to this paper's topics of alloy composition, additive manufacturing paths, the effects of heat treatment, cryogenic behavior, and industrial applications. Where the literature is very scarce, e.g. medical applications, the discussion has been made very conservatively and only reflects the range of databases and keywords that were used in this review rather than claiming the absolute absence of such studies. This procedure makes the whole reviewing process more transparent, more defensible, and more reproducible.

3 Composition and properties of invar alloys

Invar alloy is widely recognized as one of the most remarkable materials in modern materials science. It is typically composed of iron (Fe) and nickel (Ni) in a ratio of 64% Fe to 36% Ni [20–22]. A detailed understanding of the complex relationship between microstructure, properties and composition of this material provides a building block upon which optimization of Invar performance in advanced manufacturing applications. Additionally, these allow for the development of various process strategies that maximize the unique properties of Invar.

3.1 Fundamental composition and microstructure characteristics

The main chemical composition of Invar alloy centers on the critical iron-nickel ratio that was carefully optimized over many decades of materials development. Invar 36 consists of about 36% nickel with the iron balance and includes some refined control of alloying elements and impurities [23–26]. The carbon content is limited to a maximum of 0.03% and causes carbide precipitation at high temperatures, which degrades both the mechanical properties and long-term dimensional stability. Manganese is limited to 0.5%, silicon to 0.5%, sulfur to 0.01%, and phosphorus to 0.01%. Extensive research into adding various elements to the compositions showed that even small changes fundamentally alter the alloy's thermal expansion behavior and mechanical strength [13, 15, 27, 28]. Nickel content plays an important role in establishing the invar effect through the establishment of ferromagnetic behavior that underlies the unique thermal expansion properties of the alloy. Research has shown that any variation in the nickel content leads to significant changes in both the thermal expansion coefficient and the Curie temperature. The tight control of sulfur and phosphorus content in this material is critical to maintain weldability and prevent the formation of brittle phases that could affect the mechanical structure [29–32].

The microstructure of Invar alloy consists primarily of a face-centered cubic austenitic phase that remains stable across the alloy's useful operating temperature range. The austenite phase, stabilized by the high nickel content, provides the crystallographic framework within which the ferromagnetic interactions occur, with nickel atoms occupying specific lattice positions that facilitate the electron redistribution necessary for ferromagnetism [33, 34]. The grain structure of annealed Invar is typically equiaxed with grain sizes ranging from 50 to 200 µm, controlled through recrystallization during heat treatment [35]. Below the Curie temperature of approximately 279–280 °C, the Invar exhibits spontaneous magnetization with magnetic moments aligned parallel to one another, creating the internal magnetic fields that produce magnetostriction and consequently reduce thermal expansion [36]. Table 1 presents a systematic comparison of the physical and thermal properties of Invar with those of numerous substitutes used in various engineering applications.

Based on the reported properties, Invar exhibits a CTE approximately 12 times lower than that of 304 stainless steel, making it highly suitable for precision applications where dimensional stability is critical (Fig. 2). However, these come at high cost due to nickel content, lower mechanical strength, and reduced thermal conductivity that affects heat transfer during machining. Super Invar offers even lower thermal expansion but sacrifices ease of fabrication and introduces composition-dependent phase transformations that limit its applicability. Thermal expansion is optimized in Kovar to match borosilicate glass for hermetic sealing applications [37, 38].

The CTE represents a critical material property that underpins its suitability for precision applications. The linear CTE for Invar 36 is dependent on temperature, showing minimum values near room temperature, and can increase at both lower and higher temperatures. As illustrated in Fig. 3, the rapid increase in thermal expansion coefficient above the Curie temperature of 279 °C indicates the transition from ferromagnetic to paramagnetic behavior, where the material loses the spontaneous magnetization that produces the compensating magnetostriction.

The mechanical properties of Invar alloys represent a compromise between the compositional requirements for low thermal expansion, and the structural integrity demands

Table 1 Comparison of Invar alloys with competing alloys

Property	Unit	Invar 36	Stainless steel 304	Super Invar	Kovar	Carbon steel
Nickel content	%	36.0	8–10	32.0	29.0	0.1–0.2
Cobalt content	%	0.5 max	–	5.0	17.0	–
Iron content	%	63.5	71.0	63.0	54.0	99.0
Density	g/cm^3	8.05	8.0	8.12	8.3	7.85
Melting point	°C	1427	1510	1427	1420	1540
Curie temperature	°C	279	-(austenitic)	245	940	770
CTE (20–100 °C)	$10^{-6}/K$	1.2–1.5	14.7	0.3–0.5	4.57	12.0
Young's modulus	GPa	141	193	145	140	210
Yield strength	MPa	70–220	310	276	300	250
Tensile strength	MPa	480–660	515	483	520	350–400
Elongation	%	35–40	40	40	45	20–30
Thermal conductivity	W/m·K	10–13	16.2	12	17	50
Electrical resistivity	μΩ·m	0.5	0.72	0.82	0.6	0.1
Specific heat	J/kg·K	515	500	505	480	490
Relative cost	–	High	Moderate	Very High	High	Low

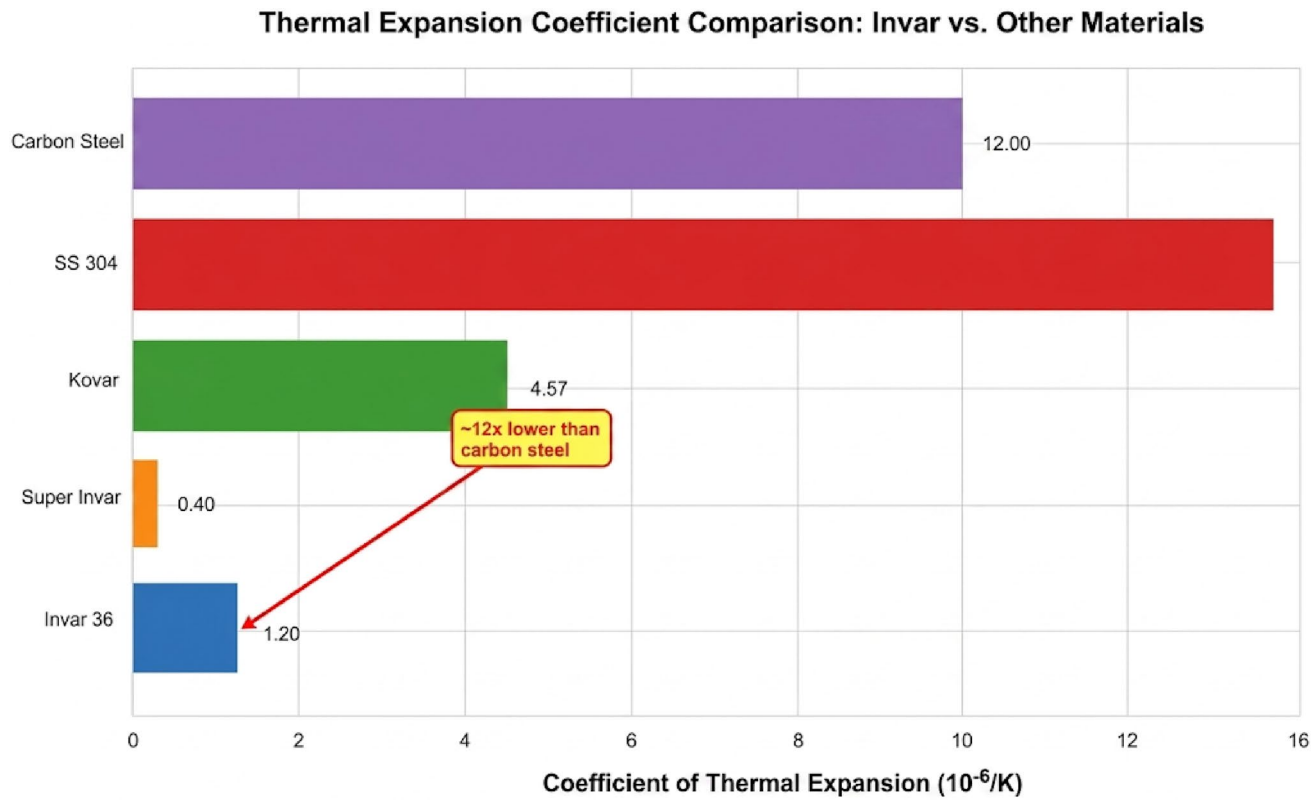


Fig. 2 Thermal expansion comparison of Invar alloys with other competing materials [39, 40]

for typical engineering applications. While this alloy offers dimensional stability, its mechanical strength is not comparable to high-strength steel or titanium alloys. Research has focused on enhancing the strength of Invar alloy while maintaining its low CTE, with studies showing methods such as cold deformation-aging to promote the precipitation of strengthening phases, resulting in significant improvements in tensile strength and elongation [42, 43]. Deformation nanostructuring by high-pressure torsion has been shown to increase the microhardness and tensile strength of Invar alloy, offering potential for improved mechanical properties [44]. The tensile properties of Invar show that it exhibits a moderate strength with excellent ductility, and its elongation indicates its capacity to withstand large plastic deformation before fracture (Fig. 4) [45–49].

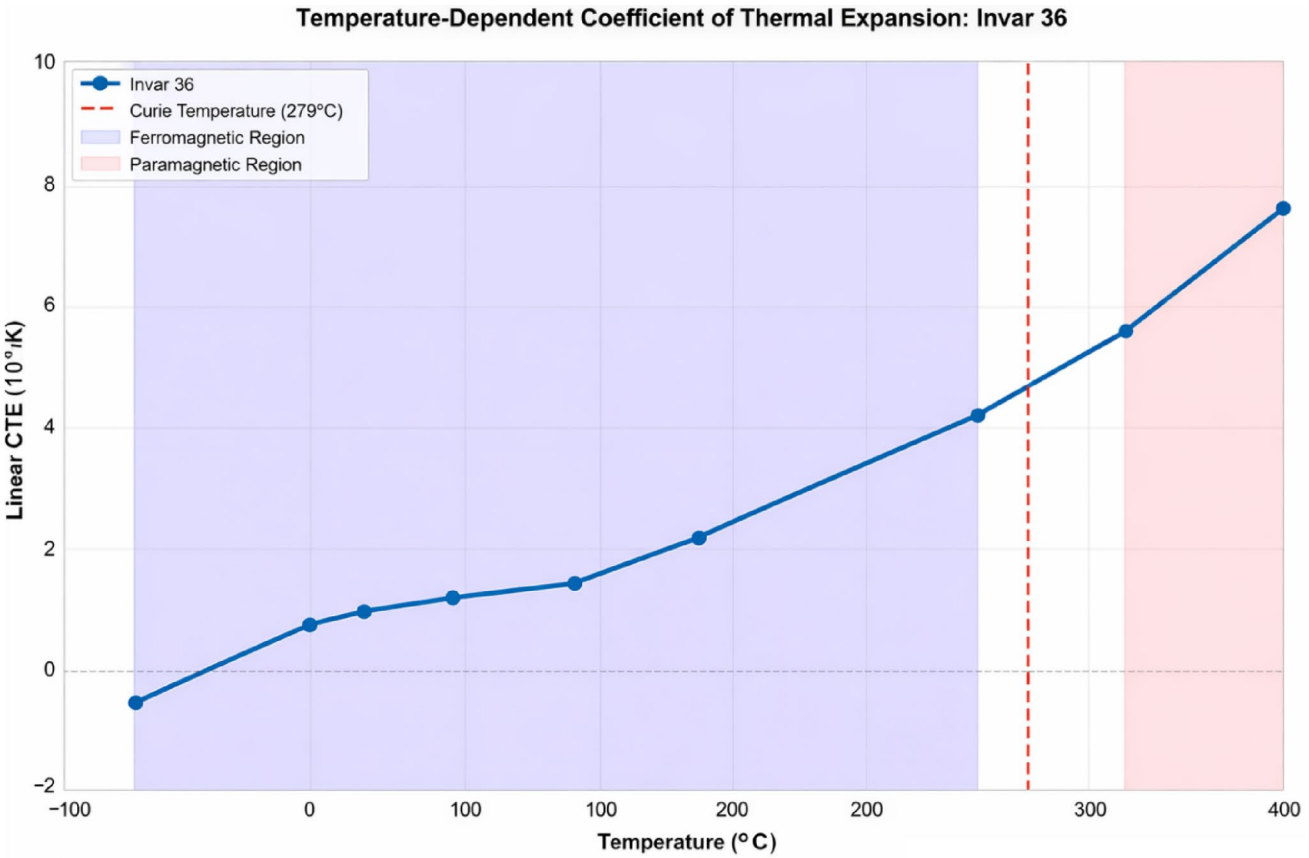


Fig. 3 Temperature-dependent thermal expansion of Invar 36 alloy. Adapted from Hitzler et al. [41]

4 AM processes of invar alloys

4.1 Overview of 3D printing techniques

According to the ISO/ASTM 52900 standard, AM technologies are divided into seven main categories: vat photopolymerization, material jetting, binder jetting, material extrusion, powder bed fusion (PBF), sheet lamination, and DED [50–52]. Of these methods, only PBF and DED can be used for metal fabrication. A review of the literature reveals that studies have been conducted on the production of Invar 36, particularly using LPBF and DED, but studies using other PBF derivatives, such as electron beam melting (EBM), are quite limited [27, 53].

The LPBF method is based on the selective melting of metal powders by depositing thin layers of material using a high-power laser beam. This method allows for the production of parts with high resolution and complex geometries. The process is typically conducted in an inert gas atmosphere (argon or nitrogen), which prevents oxidation. Due to the high cooling rates in LPBF, fine-grained microstructures are achieved, contributing to increased strength. However, process parameters must be carefully optimized to avoid defects such as thermal stresses and porosity [54, 55]. The LPBF method is particularly preferred for aerospace and mold-and-die applications because it offers high dimensional accuracy and surface quality [56].

The DED method is based on the principle of simultaneously melting metal powder or wire-formed raw material with an energy source (usually a laser, electron beam, or plasma arc) and depositing it directly onto the substrate surface. This method is suitable for high deposition rates and large-sized part production. DED is also frequently used in applications such as repairing damaged metal parts or customizing existing parts (feature addition). However, compared to LPBF, it offers lower surface roughness and dimensional accuracy. Parameters such as energy density, powder feed rate, and scanning strategy in the DED process directly affect the microstructure and mechanical properties [57, 58]. Achieving homogeneous microstructure and thermal stability in parts produced using the DED method for low-coefficient alloys such as Invar 36 is currently under research. The AM techniques used for Invar alloys are summarized in Fig. 5.

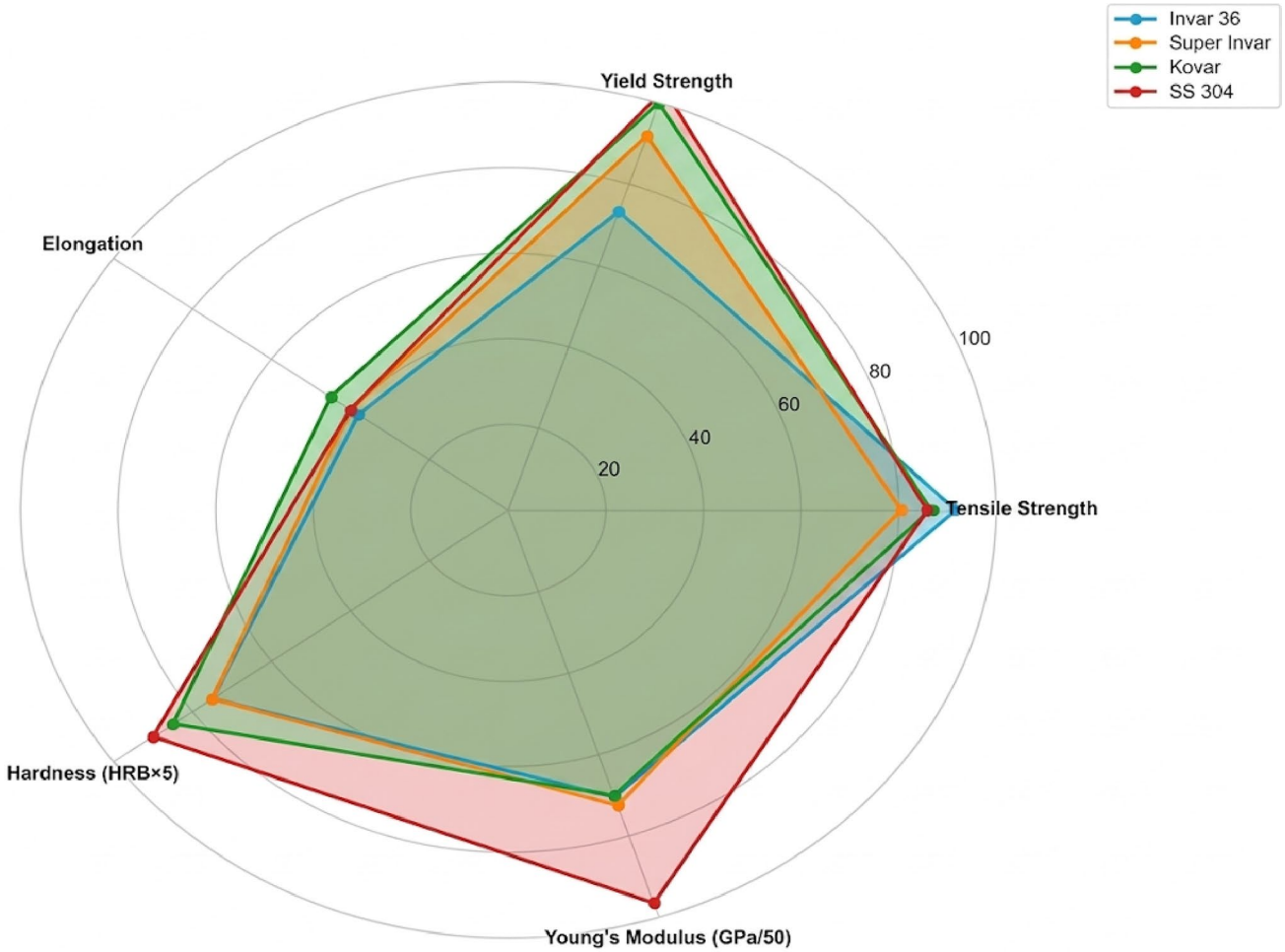


Fig. 4 Normalized mechanical properties of Invar alloy compared to other materials. Adapted from Wei et al. [49]

4.2 Process parameters and challenges

4.2.1 LPBF method

Huang et al. used the LPBF method on an EOS M290 device using a 400W YLR-400 fiber laser with a wavelength of 1064 nm and a beam diameter of approximately 100 µm. The optimum parameters were determined as follows: laser power 240 W, hatch spacing 0.15 mm, scanning speed 1025 mm/s, laser thickness 0.03 mm, and rotation angle 67°. They fabricated samples with these parameters in different orientations and investigated the microstructure, mechanical properties, and thermal expansion. The sample at the 90° orientation exhibited the highest elongation (62.70%), while the sample at the 45° orientation exhibited the highest yield strength (496 MPa). The anisotropic mechanical properties were attributed to changes in dislocation density, grain size, and intrinsic yield strength. The CTEs of Invar 36 alloy samples produced by LPBF were observed to be lower than those of conventional production processes across all temperature ranges. Since CTE is not sensitive to microstructure and is more related to magnetic properties, CTE anisotropy is not observed to be significant in the three structure directions [27].

Asgari et al. investigated the microstructure, CT and thermal expansion behavior of samples produced with INVAR 36 material using LPBF AM method on a Renishaw AM400 machine using 4 different laser powers of 250 W, 300 W, 350 W, and 400 W and volumetric energy densities of 119 (J/mm^3), 143 (J/mm^3), 166 (J/mm^3), and 190 (J/mm^3) as process parameters, respectively. LPBF-fabricated Invar samples demonstrate relative densities of 99.8%, validating the suitability of the volumetric energy density values employed in this study. At a laser power of 250 W, conduction mode is established; however, increasing the power to 300 W results in the emergence of transition mode, which exhibits characteristics of both conduction and keyhole modes. Elevating the laser power to 350 and 400 stabilizes the keyhole mode, which is characterized by goblet-shaped melt pools in the microstructure. Augmenting the laser power from 250 to 400W enhances the ⟨110⟩

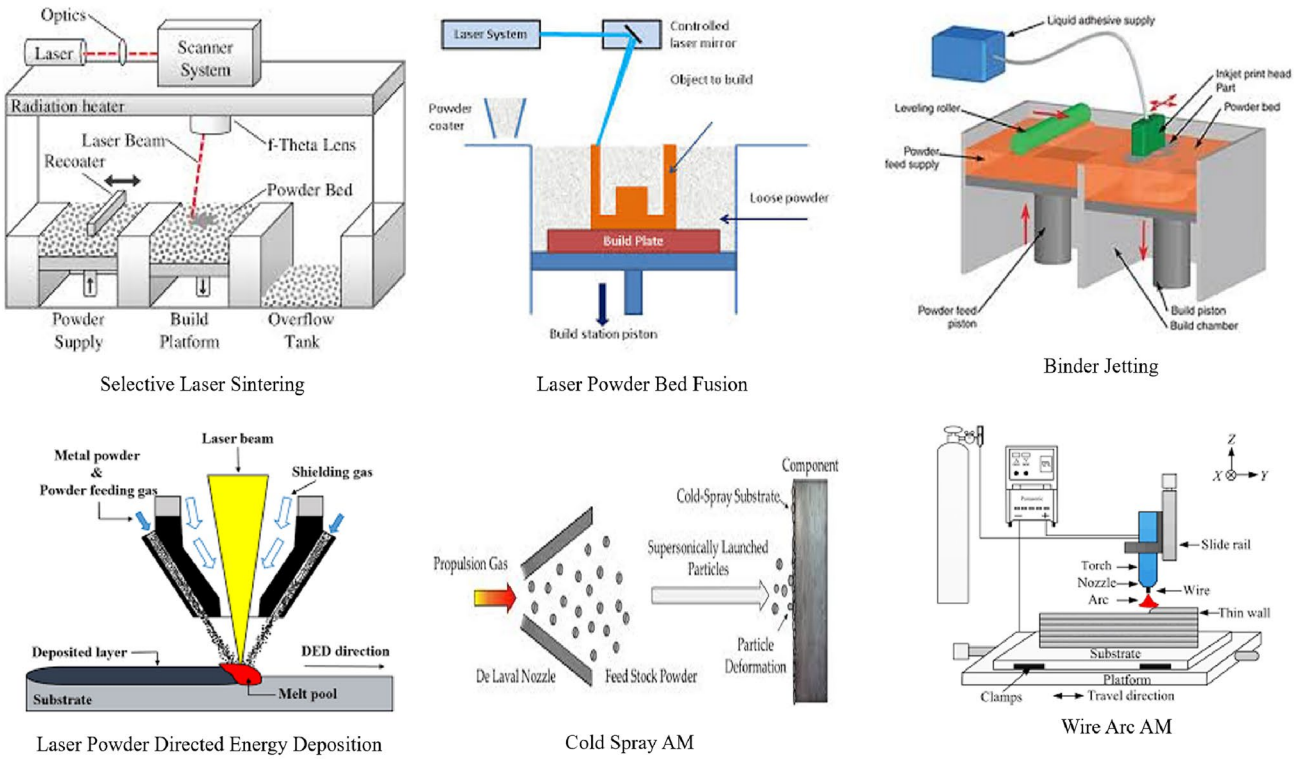


Fig. 5 Compilation of AM techniques used for Invar alloy applications. Adapted from Huang et al. [8]

texture component aligned with the building direction. The thermal expansion displacement of LPBF-fabricated Invar samples increases: (1) as porosity content decreases, and (2) with the enhancement of the ⟨110⟩ texture component along the building direction [9].

In the study by K. Wei et al. samples were produced with different volumetric energy densities using the LPBF method on a Renishaw AM250 machine using the parameters of laser power $P = 200$ W, layer thickness $t = 0.05$ mm, and hatch spacing $h = 0.125$ mm. The island scanning strategy was used in sample production. Density, hardness, tensile, and microstructure examination tests were performed on the produced samples. Since increasing exposure time and decreasing point distance increase input laser energy, which results in stable melting and thus higher density and hardness, the underlying LPBF process parameters exhibit a strong correlation with the macro characteristics. The microstructures are significantly impacted by laser energy density. Significant lack of fusion pores, unmelted powder particles, and hazy island boundaries are caused by $Ev = 23.5$ and 55.5 J/mm^3. Square islands with regular laser scanned tracks and stable bounds are formed with $Ev = 99.2$ J/mm^3. A few keyhole pores are created by $Ev = 198.4$ J/mm^3, which also causes irregularities in the laser-scanned tracks and island transfer borders. For the LPBF process using the island scanning approach, 99.2 J/mm^3 is the ideal laser energy density. Subsequently, the as-formed Invar 36 exhibits equivalent values to the conventionally produced Invar 36, including a relative density of 99.5%, Vickers hardness of 1.8 GPa, and ultimate tensile strength of 480 MPa. The γ and α phases make up the majority of the as-fabricated Invar 36. Testing temperatures of 200 °C and 600 °C cause the γ phase to coarsen, which significantly degrades the tensile characteristics [49].

Huang et al. used the LPBF method to fabricate Invar 36 using different process parameters on an EP-M650 machine tool and investigated the effects of these parameters on the microstructure, mechanical properties, and thermal expansion behavior. The laser energy used in the study was used to study the influence of each process parameter on the quality of Invar 36 alloy. A total of 25 specimens with laser power (100 W–300 W), scanning speed (800 mm/s–1200 mm/s), and hatch distance (0.06 mm–0.10 mm) were prepared. As the VED increases from 41.67 to 125.00 J/mm^3, undercooling rises, resulting in reduced nucleation rates, larger grain sizes, and a more columnar morphology. The average grain size increases from 49.80 to 147.6 μm, and the aspect ratio of the grains shifts from 3.58 to 4.71. The mechanical properties of the alloy are strongly influenced by dislocation strengthening, with the optimal mechanical performance observed at a VED of 89.29 J/mm^3, where the yield strength, ultimate tensile strength, and ductility reach values of 405.4 MPa, 489.3 MPa, and 43.3%, respectively. These properties are comparable to those achieved via traditional

manufacturing methods and heat treatment. The alloy also demonstrates an exceptional low CTE, with values complying with ASTM F1684 standards over the temperature range of 30–300 °C. Notably, porosity negatively impacts CTE, with the minimum CTE observed at a VED of 41.67 J/mm^3, where the relative density is 95.79%. The effect of porosity on CTE diminishes with increasing temperature, as the internal voids no longer provide sufficient expansion space. This study underscores the importance of controlling VED in the LPBF process to optimize the mechanical and thermal properties of Invar 36 for advanced engineering applications [8].

Lin et al. used different parameters to produce Invar 36 using the LPBF method to achieve high strength and low thermal expansion by utilizing the effects of alloying elements. First, they determined the chemical composition of the Invar alloy that provided the highest strength using the casting method, as shown in Table 2. Process parameters were laser power (P) from 200 to 400 W, scanning speed (u) from 500 to 1000 mm/s, layer thickness (t) was 30 µm, hatch distance (h) was 150 µm, and laser spot diameter was 60 µm. During manufacturing, the scanning strategy incorporated a 67° interlayer rotation, and the build chamber was purged with nitrogen gas. The study concluded that the highest strength was achieved with a density of 99.5 mm, produced with a hatch distance of 0.15 mm, a layer thickness of 0.3 mm, a laser power of 380 W, and a scanning speed of 800 mm/s. The study observed that aging at 650 °C/3 h increased yield strength by approximately 50%. Due to the opposing effects of residual stress reduction and the precipitation of strengthening elements from the matrix, the thermal expansion parameters of the produced Invar alloy exhibit little change before and after aging treatment. Under 150 °C, the heat-treated alloy's CTEs maintain a low value ($<2\times10^{-6}$ °C^{-1}), indicating sustained dimension stability [59].

Wegener et al. produced samples using the LPBF method using a chessboard scanning strategy on a TruPrint 1000 device with a layer thickness of 30 µm, a hatch distance of 0.105 mm, a fiber laser operating with a spot size of 75 µm at a speed of 900 mm/s and a power of 200 W, resulting in an energy density of approximately 70.5 J/mm^3. The microstructure, tensile strength, fatigue, hardness, and thermal expansion behavior were investigated. The resulting grain sizes were observed to be an average of 75 µm in production direction. X-ray CT testing yielded a porosity ratio of 0.4% and a density ratio of 99.6%. The hardness distribution of the parts is homogeneous, with no gradient in relation to the build height, due to the robustness of the applied process parameters. Monotonic tensile tests show a ductile material behavior, with a yield strength (YS) of 310 MPa and ultimate tensile strength (UTS) of 445 MPa. Fracture surfaces exhibit a characteristic dimple-like appearance with a cup-and-cone shape. The material shows minimal cyclic softening under cyclic deformation, with a high degree of reproducibility and damage tolerance, evidenced by consistent stress amplitude and cycle-to-failure data. Half-life hysteresis loops demonstrate perfect Masing behavior, meaning the microstructure evolves similarly regardless of strain amplitude. Post-fatigue analysis reveals crack initiation on the machined and ground surfaces, with minor internal porosity detected, likely due to hollow powder particles and keyholing effects. Despite these process-induced defects, the alloy exhibits damage-tolerant behavior under cyclic loading. In terms of thermal properties, the LPBF-processed Invar alloy demonstrates a low CTE of 1.8×10^{-6} K^{-1} between 0 and 100 °C, comparable to conventionally processed Invar, and maintains this low thermal expansion up to 180 °C [60].

Table 2 Chemical compositions of high-strength Invar alloy powder

Elements/%						
Fe	Ni	Co	Mn	Cu	V	C
Balance	31.53	3.47	0.56	0.50	1.76	0.075

Yang et al. investigated the high-temperature tensile behavior of Invar 36 alloy produced with LPBF using X-ray CT. They used three different volumetric energy densities: Ev = 74.1 (inadequate energy input), 148.2 (optimum energy input), and 185.3 J/mm^3 (excessive energy input) on a Renishaw AM250. They performed porosity measurements, microstructure examinations, and tensile tests under X-ray CT on samples produced with three different parameters. Consequently, the high-temperature tensile behavior of Invar 36 alloy is notably affected by the lack-of-fusion (LOF) pores. The substantial volume of these pores reduces the load-bearing area, resulting in diminished strength. LOF pores at the edges possess high-stress concentration, providing more paths for crack propagation and emerging as the sites of crack initiation. Their small spacing, elongated shape, and perpendicular orientation to the loading direction contribute to stress concentration and promote crack propagation, ultimately leading to premature failure. Furthermore, it is noted that higher laser energy density resulted in larger cell sizes, thereby decreasing the yield strength of the Invar 36 alloy [61].

4.2.2 DED method

Veiga et al. used Wire Arc Additive Manufacturing (WAAM) technology, Addilan V0.1, equipped with an EWM brand generator, Titan XQ 400 AC puls DW and an M drive 4 Rob5 XR RE wire feeder, and the machine has been equipped with a laser profilometer per beam, Laser Scanner Q4 Series, and with an infrared measurement camera TACHYON 1024 microCAMERA Uncooled MWIR camera

IP-67 up to 1 kHz frame rate. A total of 9 test with Wire feed (4;10;16 m/min), deposition rate (2.2;5.5;8.8 kg/h), traverse speed (40–320 cm/min), ratio (5;7.5;10), current (109.8–448.43 A), and voltage (19.29–36.83 V) were performed. As a result of production and tests, deposition conditions were optimized for bead geometry, resulting in a symmetry coefficient nearing 0.99 for most tested conditions. The wall geometry, measured using a passive macroscopic image, achieved a mean symmetry coefficient of 0.998, indicating a close approximation to pure symmetry [62].

Jiao et al. conducted a WAAM system by using a KUKA KR20 industrial robot as a manipulator and a welding system with Fronius CMT 4000 R advanced power source. The feeding wire used was an Invar wire with a diameter of 1.2 mm, fed at a rate of 8.0 m/min. Argon gas (99.99% purity) was used as the shielding gas at a flow rate of 20 L/min to ensure a stable and contamination-free arc environment. The substrate material was 316L stainless steel, preheated to 100 °C to improve adhesion and reduce thermal stress during deposition. The torch traveling speed was maintained at 0.25 m/min, while the deposition current and voltage were set to 180 A and 15.6 V, respectively, providing stable arc conditions for uniform layer formation. Some samples are conducted stress relief heat treatment that the heating rate was set at 5 °C/min, the heat treatment procedure used was as follows: The heating rate during the treatment was 5 °C/min, following a procedure comprising four steps: (1) heating from room temperature to 830 °C and holding for 0.5 h; (2) water quenching; (3) heating to 310 °C, then air cooling to room temperature after 1 h; (4) heating to 95 °C and aging for 48 h. After production, microstructure examinations, tensile tests, impact, and thermal expansion behaviors were performed. The microstructure of the as-deposited (AD) and heat-treated (HT) samples was characterized by columnar γ grains adorned with the primary phase and nanoscale dispersoids. The precipitated phases were characterized as (Nb, Ti)C (0.5–1 μm) and NbC (30–500 nm). The anisotropy of the microstructure results in the strength of samples evaluated along the wall direction (WD) being superior than that of samples tested along the building direction (BD), both prior to and following heat treatment. The ultimate tensile strength of the HT sample measured along the width direction is 540 MPa, surpassing that of its counterparts in the existing literature. The augmented nanoscale NbC is the primary factor contributing to the enhancement of strength following heat treatment. The CTE of the AD samples is anisotropic owing to the anisotropy of the microstructure. The augmentation of NbC precipitation following heat treatment diminishes the Ni concentration in the matrix from 36.4 to 35.72% (approaching 36%), hence mitigating distortion inside the matrix. The average CTE for the HT samples was 1.13×10^{-6} C^{-1} (0–100 °C), representing the lowest value reported in the literature for WAAM Invar components [63].

Chen et al. used Cold spray (CS) AM to create the Invar 36 alloys. The mechanical characteristics, thermal expansion, and microstructural evolution under as-sprayed (AS) and HT conditions were all systematically investigated. Analysis using X-ray diffraction (XRD) and inductively coupled plasma atomic emission spectroscopy (ICP-AES) reveals no changes in element content, oxidation, or phase transition. In the helium-made sample under as-sprayed conditions, the XCT revealed a nearly entirely dense structure with a porosity of 0.025%, while the nitrogen-generated samples created at 5 MPa and 800 °C display more irregular pore flaws. Because of the greater degree of plastic deformation, the He-AS sample exhibits a more noticeable grain refinement than the nitrogen samples. Grain growth, interparticle diffusion, and the development of annealing twins were all enhanced by the post-heat treatment. The nitrogen samples had lower CTE values (1.53×10^{-6}/°C) between 25 and 200 °C when compared to those made by casting and laser AM. Between 25 and 200 °C, the He-AS samples showed a pronouncedly negative CTE value. This could be because, during the CTE test, the substantial compressive residual stress (− 272 MPa) compensated for its displacement with an increase in temperature. There is a noticeable balance between strength and ductility in the N_2-HT and He-HT Invar 36 samples. To sum up, the CS technique may be a viable way to create the Invar 36 component with excellent mechanical and thermal performance [16].

Bobbio et al. deposited the gradient sample utilizing a DED technique (RPM 557 Laser Deposition technique). The square post samples, featuring a base area of 15 mm by 15 mm, were produced utilizing a YAG laser, functioning at a power of 900 W and a scanning velocity of 12.7 mm/s. The hatch angle was 90 degrees, indicating that the scanning direction rotated 90 degrees for each layer. The layer height was 0.38 mm, while the hatch width was 0.58 mm. The manufacturing procedure was executed in an argon environment. The manufacturing procedure resulted in detrimental phases due to the compositional blending of Ti-6Al-4 V and Invar, causing cracking in the final deposited component. Intermetallic phases (FeTi, Fe_2Ti, Ni_3Ti, and $NiTi_2$) were experimentally seen in the gradient region and were deemed responsible for the cracking of the functionally graded material (FGM) during manufacturing. The Ti-6Al-4 V to Invar FGM exhibited morphological defects such as material overflow and macroscopic cracking, rendering the linear gradient pathway unsuitable for applications. A low melting point composition, determined by CALPHAD-based thermodynamic calculations, was found to cause a significant drop of approximately 650 K in both solidus and liquidus,

leading to material overflow at around 12–18 vol% Invar [64].

Aldalur et al. produced the samples utilizing the Addilan WAAM machine v0.1 for experimentation, which enables the fabrication of components through both Gas Metal Arc Welding (GMAW)-based and Plasma Arc Welding (PAW)-based WAAM technologies. The machine is outfitted with the Titan XQ 400 AC puls (EWM) welding source for GMAW. The thermal and microstructural characterizations of Invar 36 alloy produced using two methods of WAAM technology (PAW-based and GMAW-based) are presented to validate the WAAM technology. In PAW technology, the heat input was significantly higher than in GMAW due to low arc efficiency, resulting in almost double the temperature during deposition. Dilatometry results showed that Invar made using GMAW exhibited a CTE similar to reference laminated material, indicating its suitability for manufacturing parts with good thermal behavior. In contrast, PAW-manufactured samples had higher CTE values. Curie temperatures varied among processes, with GMAW yielding higher values than PAW. SEM analysis revealed no macrostructural defects in both method; however, PAW samples had a greater concentration of niobium carbides. Overall, GMAW-based WAAM technology produced Invar 36 efficiently, maintaining microstructural integrity [65].

Ye et al. used Gas Tungsten Arc Welding (GTAW)-type WAAM equipment consisted of a three-axis CNC machine tool, a gas tungsten arc welding, a wire feeding mechanism, a workbench, a Tungsten Inert Gas welding (TIG) power source, and a control system. WAAM is utilized to produce a thin-walled rectangular component made of super-invar alloy. The microstructure features cellular sub-grains exhibiting diverse morphologies inside the epitaxially formed columnar crystals. The finite element modeling findings indicate that the G (temperature gradient)/R (solidification rate) ratio during the deposition process is calculated to be 1.59×10^8 K·s·m^{-2}, which correlates with the columnar cellular microstructure. The droplet transfer mode during WAAM is the liquid bridge transition. The mechanical parameters of the specimens exhibit anisotropy, with longitudinal samples outperforming transverse samples; the ultimate tensile strength (UTS) is 398.8 MPa, the yield strength (YS) is 291.4 MPa, and the elongation is 40.8%. The CTE is quantified as 0.265×10^{-6} K^{-1} within the temperature range of 20–100 °C. The results serve as a benchmark for the rapid production of super-invar alloy components by WAAM [8].

4.3 Primary advantages, limitations, and AM strategy recommendations for invar alloys

Invar 36 is a special Fe–Ni alloy known for its low thermal expansion and high dimensional stability [18]. This material offers significant structural and functional properties comparable to traditional manufacturing methods through AM. The AM process allows for the production of complex geometries, increasing design freedom and significantly reducing material waste. Furthermore, the ability to control microparticle layer by layer during production allows for the achievement of targeted mechanical and thermal properties. This is a significant advantage for alloys with high microstructures like Invar 36 [12, 66].

Another significant advantage of AM is the ability to integrate and customize parts. Producing multi-part systems in one piece reduces both assembly time and manufacturing costs. Furthermore, thanks to the high geometric accuracy and homogeneous microstructure, Invar 36 parts produced using AM can exhibit mechanical strength and low thermal expansion properties similar to those produced using traditional methods. Furthermore, by optimizing production parameters (power, scanning speed, energy density, etc.), density and surface quality can be increased, and microporosity can be minimized [6, 67].

However, the production of Invar 36 using AM has some limitations. Residual stresses resulting from high temperature gradients and rapid solidification can lead to part deformation or cracking. Porosity, keyhole effects, and voids resulting from powder morphology can also negatively impact the material's mechanical and thermal performance. Furthermore, surface roughness is typically high, requiring post-processing (e.g., grinding or polishing). The process's energy consumption and equipment costs are also higher compared to traditional manufacturing [39, 68].

In conclusion, Invar 36, produced through AM, has great potential in terms of high-dimensional stability, design flexibility, and microstructure control. However, technical challenges such as controlling residual stress, reducing porosity, and improving surface quality are key issues that must be addressed before the process can be widely adopted at an industrial scale. Process optimization, and advanced heat treatment techniques will reduce these limitations, allowing Invar 36 to be safely used in high-precision applications using AM [12].

There are many variables involved when choosing an AM method for Invar 36, such as the geometric complexity of the part, the scale of the part, and the part's need to maintain the alloy's near-zero CTE. If high-precision applications are to be used, LPBF provides a viable option to produce complex, low-weight aerospace brackets and optical housings with a resolution of 20–50 microns, though controlling the laser energy density will be important in order not to vaporize Ni [14, 69]. If the primary engineering requirement is large-scale production, such as five-meter molds for the composite tooling industry, WAAM is the superior choice; while it results in coarse, anisotropic grain structures, its

Table 3 Comparative analysis of AM techniques for invar alloys: processing characteristics, microstructural features, and application suitability

Feature	LPBF	BJT	WAAM (Arc-DED)	CSAM
Porosity/density	High (>99.5%)	97–99% post-sinter	High; prone to gas	Very high (>99%)
Texture/anisotropy	Columnar grains	Equiaxed	Massive columnar	Deformed
Ni evaporation risk	High	Low	Moderate	Zero
CTE retention	Sensitive (<1.5)	Excellent	Good (~0.26)	Best (~0.5)
Mechanical Perf	High YS; low EL	Moderate	High ductility	High hardness
Post-treatment	Stress relief	Sintering	Heavy machining	Annealing
Best application	Complex aero parts	Isotropic small parts	Large-scale tooling	Repairs/Coatings
Main limitation	Residual stress	20% Shrinkage	Heat distortion	Line-of-sight only

Table 4 Process–structure–property–application map for AM of invar alloys [70–73]

AM route	Dominant microstructural feature	Property consequence	Suitable application
LPBF	High dislocation density; ultra-fine subgrains; crystallographic texture	Exceptional strength; risk of Ni-loss (vaporization); low CTE if chemistry is maintained	Precision aerospace; complex cooling channels; high-end tooling
WAAM	Large-scale columnar grains; significant anisotropy; low thermal gradients	High deposition rates; scalable but requires heavy post-processing (heat treat) for isotropy	Large-scale molds; structural maritime components; heavy tooling
DED/LMD	Sharp thermal gradients; epitaxial growth; compositionally graded zones	Ideal for functional grading (FGM); moderate surface finish; excellent for local reinforcement	Component repair; hybrid manufacturing; graded transition joints
CSAM	Solid-state bonding; high retained composition; severe plastic deformation	No melting (no Ni-loss); high compressive residual stress; low ductility without annealing	Dimensionally stable parts; protective coatings; repair of heat-sensitive alloys

deposition rates are nearly 50 times faster than beam-based methods [17].

On the other hand, if thermal stability and chemical integrity are the most important aspects, cold spray (CS) AM also has an advantage as a solid-state process. Since it does not melt at all, CSAM does not have a risk of depleting Nickel, nor does it change the composition of the feedstock, thereby making CSAM more suitable for both repairs and for making very large block preforms [16]. If batch producing small parts is to be accomplished and multi-dimensional stability (even before sintering) is an absolute requirement, binder jetting (BJT) would be the recommended method; the furnace based sintering cycle will create more equiaxed, isotropic grains than other (melt-based) processes that will create a columnar type of grain structure. Ultimately, the final choice of technology should be able to balance the complexity of LPBF; the enormous size of WAAM; and the chemical precision of either CSAM or BJT in order to ensure that the "invar effect" is maintained in the intended application. Table 3 provides a comparative summary of key AM methods for Invar alloys, pointing out variations in porosity/density, texture and anisotropy, nickel evaporation risk, CTE preservation, mechanical properties, post-processing needs, and common uses [14, 16, 69].

A clear mapping between additive manufacturing routes, microstructural features, and resulting properties is critical for guiding material design and application-specific selection. Table 4 explains these interdependencies for Invar alloys [70–73].

5 Heat treatments of invar alloys

Fe–Ni alloys are important engineering materials that exhibit high permeability and magnetic induction compared with other soft magnetic materials [74]. Invar's very low CTE makes it preferred in applications requiring precision and dimensional stability [75, 76]. Heat treatments are applied to control the microstructure, mechanical properties, and magnetic/thermal expansion behavior of Invar. Commonly used heat treatments include solution annealing, stress relief annealing, homogenization, aging, and post-deformation heat treatment.

5.1 Types and purposes of heat treatments

When considering the applied heat treatments, solution annealing is performed at approximately 1000–1100 °C followed by quenching. This process stabilizes the austenite phase and maintains a low coefficient of expansion. Stress-relieving annealing is performed at 250–400 °C to reduce residual stresses and increase dimensional stability. Aging heat treatment is applied at 150–300 °C to improve magnetic properties and examine Curie temperature behavior. This also increases mechanical strength. Because higher temperatures, such as 1000–1100 °C, lead to grain growth, some studies have selected a more controlled temperature of 850 °C for homogenization. The fact that the Invar remains in the austenitic region, but grain growth is not as rapid, provides a mechanical advantage. Prolonged holding at 850 °C breaks down chemical segregations, removes carbide/phase residues, and results in a more homogeneous austenite. However, 850 °C may not always be sufficient

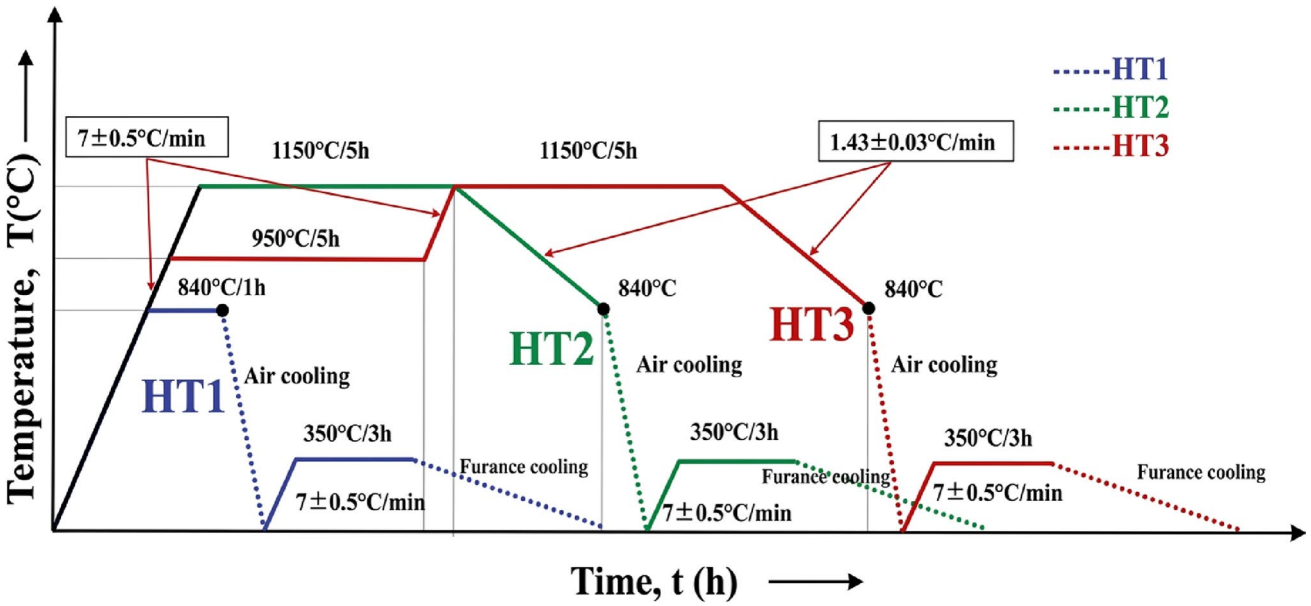


Fig. 6 Heat treatment cycles of samples subjected to a multi-stage heat treatment process [79]

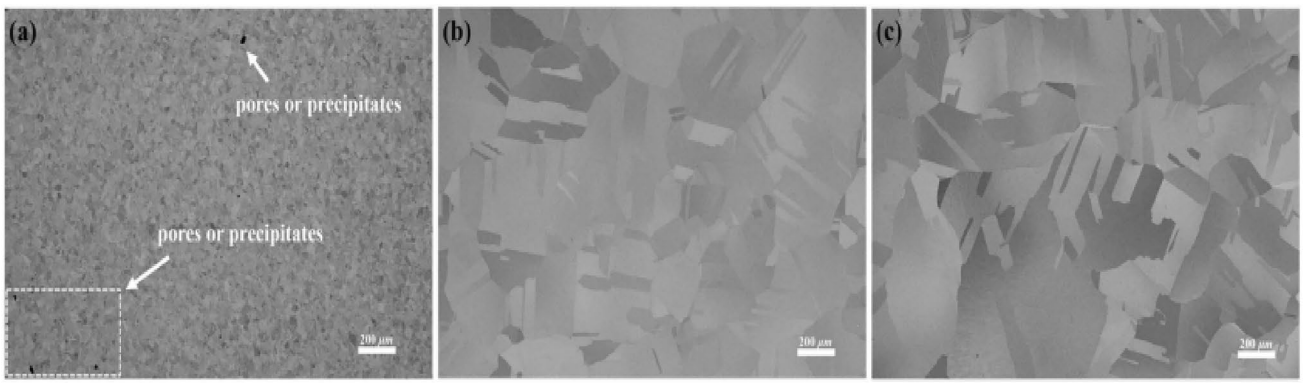


Fig. 7 Microstructures of samples **a** low temperature annealing **b** single stage high temperature annealing, and **c** step high temperature annealing [79]

to resolve segregations. Therefore, solution annealing at a higher temperature followed by quenching can provide an advantage compared to the previous case [77]. Dislocation theory explains this situation [78]. Stress relief heat treatments performed after cold forming can provide both dimensional stability and strength increases. In a different study, the low-temperature heat treatment process involved holding samples at 840 °C for 1 h, then air-cooling, and then stress relieving at 350 °C for 3 h before cooling in an oven. A single-step high-temperature annealing process involved stress relieving at 1150 °C for 5 h, followed by stress relieving at 350 °C for 3 h. In a step-by-step high-temperature annealing process, heat treatment was carried out at 950 °C for 5 h, followed by stress relieving at 1150 °C for 5 h, and then stress relieving at 350 °C for 3 h. When the surface morphology, phase ratios, crystallinity size, elastic modulus, magnetic properties, and coefficient of expansion values of the samples were examined, it was concluded that the samples subjected to the gradual high-temperature annealing process exhibited high permeability and very low coefficient of expansion. The applied heat treatment cycle is shown in Fig. 6 [79].

5.2 Effects of microstructure on properties

When the microstructures were examined after the heat treatment routes performed by Li et al. differences were observed, as shown in Fig. 7. Studies have shown that low-temperature heat-treated samples had some pores or precipitates on their surfaces, with grain sizes of approximately 20 µm. As the heat-treatment temperature increased, the grain size of the single-stage high-temperature annealed sample increased significantly, reaching approximately 200 µm, and pores and precipitates completely disappeared.

In the stepwise high-temperature annealing process, the grain size, porosity, and precipitates showed microstructural results similar to those of the single-step high-temperature annealed sample. XRD analysis of these samples showed that the phase compositions were not affected by changing annealing temperatures and modes [79]. Furthermore, the results show that the phases in Invar 36 alloy are not affected even by varying quenching temperatures. All samples were found to have a γ phase and a more regular magnetic configuration.

Today, Invar 36 alloy plays a significant role in magnetic applications compared to other low-expansion materials [80]. However, due to the complexity of magnetism, new efforts are underway to improve the magnetic properties of Invar 36. Annealing, the most decisive treatment for Invar 36, plays a significant role in improving its magnetic properties. Therefore, developing various heat treatment processes for a high-performance Invar alloy plays a significant role in improving the material. Studies were conducted to investigate the effect of heat treatment after Hot Isostatic Pressing (HIP) and LPBF during production using AM instead of traditional methods on the porosity and microstructural evolution of Invar 36. It was found that the applied heat treatment did not cause significant changes in the microstructure, HIP closed some of the pores but caused coarsening of the α precipitates, especially at the grain boundaries, during the subsequent slow cooling. However, although HIP closed most of the pores in the samples, it did not improve the tensile properties. All samples treated with LPBF and HIP became brittle [14]. In a study in which cold-rolled Invar thin sheet material was annealed at 400 °C, 500 °C, 700 °C, 800 °C, and 900 °C, the grain structure with high intergrain irregularities in the microstructure of the cold-rolled sample was characterized. Below 800 °C, no recrystallization occurred, and above 800 °C, clear signs of recrystallization were seen, such as equiaxed grains with low intra-grain irregularities. Complete recrystallization was observed at 900 °C. When the mechanical properties after these heat treatments were examined, it was observed that after full recrystallization at 900 °C, a further improvement in ductility occurred together with a decrease in yield strength [81]. The recrystallization temperature of Invar is generally above 650 °C due to the cold-rolling reduction [81]. Moreover, for Invar alloys above 600 °C, evidence of hardness recovery can be observed depending on the degree of cold-rolling reduction [82]; this explains the absence of a pronounced indication of recovery. The lack of recrystallization at certain temperatures in this study further substantiates this observation.

Optimization studies of heat treatment parameters to be applied during or after the AM process are being carried out. The superior thermal management properties of Invar alloys will facilitate their wider use and adoption in the industrial field. As a result of the obtained studies, it creates a broad potential for researching and developing innovative methods to ensure the integration of modern heat treatment technologies with current alloy design approaches [83]. The summary of studies covered Invar alloys and AM methods applied, parameters before and after heat treatment, and final applications (Table 5).

6 Cryogenic treatment of invar alloys

Invar's mechanical limitations, such as low hardness, corrosion formations at high salt conditions, and relatively poor wear resistance, limit its performance, particularly when used in cryogenic environments. Recent research has examined the effects of cryogenic treatments on wear resistance, microstructure, fatigue behavior, and dimensional stability.

6.1 Effects on microstructures

The typical microstructure of Invar at room temperature is a single-phase γ (FCC) Fe–Ni solid solution, containing no phases other than small amounts of impurities including carbides or oxides. Cryogenic treatments applied to this material generally change the grain size and orientation. In addition, it can also change the state of defects that can be observed by TEM, such as dislocation density and stacking faults [89, 90]. When Invar samples were tested at − 196 °C with different surface micro-texturing methods, it was reported that laser-created micro-channels further reduced the friction [76]. It was observed that cryogenic treatment applications contributed to the stability of the grain structure [89]. Studies have shown that cryogenic treatment does not cause phase transformation in the microstructure. A decrease in Ni content increases the martensitic transformation temperature. It has been observed that martensitic transformation does not occur even at liquid He temperature (4 K) [91].

6.2 Enhancements in physical properties

Invar 36 alloy has been shown to exhibit excellent tribological properties with a coefficient of friction (COF) value decreasing gradually from 20 to − 78 °C and reaching a minimum value at − 196 °C when the temperature drops to − 196 °C [76]. Welded joints of Invar materials used in cryogenic tank structures were subjected to fatigue testing at − 163 °C, and the strength of thin-section welded joints was evaluated with the effective notch stress approach [89]. Cryogenic liquid nitrogen cooling of Invar 36 alloy was used, and by applying this process in the cutting zone during machining, it was achieved to reduce surface roughness

Table 5 Invar alloys, AM methods, heat-treatment effects, and primary applications

References	AM method	AM process parameters	Properties before heat treatment	Heat treatment method and conditions	Properties after heat treatment	Key findings	Applications/ relevance
[28]	LPBF	LP 250–400 W; layer 30–50 µm; ED 55–148 J/mm^3	Columnar grains; Ti (2 at%) promotes equiaxed grains; YS 357–383 MPa, UTS 440–458 MPa, EL 28–38%	N/A	N/A	Ti addition forms nano-oxides, suppresses SiO_2, increases strength (~100 MPa) while maintaining low CTE and ductility; reduced layer thickness lowers porosity	High-precision structural components
[14]	LPBF	LP 400 W; scan 1800–4300 mm/s; Ar atmosphere	Columnar γ-grains with α-precipitates; low porosity; build-direction anisotropy; CTE ≈ 2×10^{-6} K^{-1}	Annealing + aging 830 °C WQ → 570 °C AC → 95 °C soak	Mechanical properties largely unchanged; minor α coarsening; slight CTE improvement	Heat treatment stabilizes CTE but quenching induces interlayer cracks; HIP reduces porosity but weakens GBs	Aerospace, optics, electronics, cryogenics
[39]	LPBF	LP~190 W; layer 20 µm; raster scan	Columnar grains (200–300 µm); high strength; negative CTE due to residual stress	Stress relief 850 °C × 1 h (Ar)	Residual stress relieved; CTE increases slightly; anisotropy remains	LPBF Invar retains low CTE and mechanical performance comparable to wrought Invar	Precision instrumentation, aerospace tooling
[60]	LPBF	LP 200 W; scan 900 mm/s; layer 30 µm	N/A	Multi-step furnace-cooled anneal 850 → 650 → 250 °C (stepwise FC)	Bimodal grains; YS 310 MPa; UTS 445 MPa; EL 43–47%; stable CTE	Annealing relieves stress and improves ductility and fatigue stability without degrading CTE	Cyclically loaded industrial components
[84]	LPBF	LP 240 W; scan 700 mm/s; ED ≈ 95 J/mm^3	Epitaxial columnar growth; porosity decreases with ED; anisotropic strength	N/A	N/A	Higher energy density reduces porosity and improves strength; corrosion resistance retained	High-precision thermal-stable parts
[9]	LPBF	LP 250–400 W; ED 119–190 J/mm^3	>99.8% density; columnar γ-FeNi; stronger ⟨110⟩ texture at high LP	N/A	N/A	Increasing LP reduces porosity, shifts melt mode to keyhole, maintains low CTE up to 300 °C	Aerospace and cryogenic optics
[85]	LPBF (multi-material)	LP 125–285 W; ED 23–314 J/mm^3	Low ED causes porosity; high ED improves melting and bonding	N/A	N/A	Energy density governs defect formation and interlayer bonding	Aerospace, automotive, electronics
[86]	LPBF (lattices)	LP 150 W; scan 800 mm/s; TPMS designs	Dense equiaxed/columnar grains; high energy absorption	N/A	N/A	TPMS lattices show high toughness, low CTE, and excellent damping with grain-driven anisotropy	Lightweight, vibration-damping structures
[66]	WAAM	150 A; 20 V; Ar shielding	Alloying refines grains; strength nearly doubled; toughness improved	N/A	N/A	Cr–Mo–V–N alloying significantly enhances strength and impact resistance while preserving low CTE	Cryogenic, aerospace, oil & gas
[17]	WAAM	Pulsed arc; hot-wire feed	N/A	Solution + aging 840 °C WQ → 315 °C AC	Uniform hardness; ductile fracture; ultra-low CTE	Columnar cellular growth causes anisotropy; magnetostriction dominates CTE	Precision optical and aerospace components

Table 5 (continued)

References	AM method	AM process parameters	Properties before heat treatment	Heat treatment method and conditions	Properties after heat treatment	Key findings	Applications/ relevance
[16]	Cold Spray (CSAM)	N_2 or He gas; solid-state deposition	Near-full density; high compressive stress; low ductility; negative CTE (He)	Annealing 800 °C × 3 h (Ar)	Grain growth; stress relief; ductility restored; stable CTE	Heat treatment converts brittle deposits into balanced strength–ductility material	Dimensional-stability components
[87]	LMD	LP 700–1000 W; scan 300–600 mm/min	Graded grains; UTS up to ~ 590 MPa; build-direction dependence	N/A	N/A	Back-and-forth scanning improves strength; performance exceeds cast Invar	Precision and cryogenic applications
[29]	Laser SDM	2000 W Nd:YAG; Invar–TiC powders	TiC increases hardness and strength; ductility decreases	N/A	N/A	Invar–TiC composites maintain low CTE with enhanced wear resistance	Rapid tooling, high-performance parts
[88]	LSF	2000 W laser; 300–1000 mm/min scan	Columnar dendrites; higher speed improves strength and ductility	N/A	N/A	Optimal scan speeds reduce cracking while maintaining low CTE	Aerospace, electronics, precision manufacturing
[52]	Binder Jetting	50 µm layers; 90–93% green density	High surface porosity; rough surface	HIP + polishing 1100 °C, 100 MPa, 2 h	99.8% density; ~ 1 µm Ra surface	HIP eliminates porosity; post-processing enables optical-grade surfaces	Space optical components

and tool wear by approximately 25% [92]. In a different study, when the tensile strength of welded Invar alloy at -163 °C was examined, it was observed that the order of strength was HAZ (heat-affected zone) < weld core/nugget (WN) < base material (BM) [90].

7 Applications of invar alloy across various industries

Invar alloy is a valuable material famous for its very low CTE in the vicinity of room temperature. Consequently, it is the perfect material for use in any place where temperature changes and thus the stability of dimensions is necessary. In the last decade, Invar's use has expanded in aerospace, electronics, precision metrology, cryogenics, and specialty tooling. Key research has focused on new Invar-based composites, AM, and thermal treatments to enhance stability. Each application area is discussed below, accompanied by examples (Fig. 8).

7.1 Aerospace and space systems

In aerospace, Invar is used for precision support structures, optical benches, and tooling where thermal deformation must be minimal. For example, NASA's James Webb Space Telescope (JWST) Integrated Science Instrument Module uses a "special invar and composite truss structure designed for exceptional optical stability" [93]. The science instruments in JWST operate at cryogenic temperatures (40–6 K), so the Invar frame keeps the optics aligned despite thermal cycling [93]. In practice, Invar bonding pads on Zerodur mirrors showed < 5 nm RMS shape change over a 28 K span [94], illustrating Invar's ultra-stable behavior. In addition, aerospace manufacturing exploits Invar tooling for composite parts. Recent work demonstrates that Invar 36 can be produced by WAAM for large aerospace molds and dies [62]. The low-expansion Invar face sheets and backing structures are candidates for 3D-printed composite tooling, greatly reducing lead times [95].

7.2 Electronics and semiconductor manufacturing

In electronics, the stability of Invar is the main factor that increases the reliability of precision assemblies. One of the most noticeable instances is Cu–Invar laminates for the advanced circuit boards. Copper–Invar–copper (CIC) substrates are a mixture of Invar's almost zero CTE and copper's conductivity. A recent study of 50:50 Cu/Invar composites notes they have great potential to be used as novel electronic packaging materials due to enhanced thermal conductivity and still-low expansion [96]. This mitigates solder fatigue



Fig. 8 Various applications of Invar **a** pendulum clock, **b** measuring tape, **c** boiler tubes, **d** bimetallic strip, **e** 3D printed Invar for aerospace composite mold, **f** shadow masks in TV screens, **g** Invar conductor of power transmission lines, **h** LNG and Cryogenic applications, **i** bimetallic thermometer, and **j** Invar part and components. Adapted from publicly available domain figures

caused by CTE mismatch between chips ($\sim 7 \times 10^{-6}$/K) and standard epoxies ($12–16 \times 10^{-6}$/K) [97]. In semiconductor equipment (lithography stages, alignment systems), Invar variants (including new non-magnetic alloys) are used to minimize thermal drift during operation. Low-CTE Invar parts (e.g., optical mounts, wafer chuck supports) reduce thermal errors in semiconductor lithography tools. Recent SPIE work on non-ferromagnetic Invar alloys targets even better stability for optics in semiconductors.

7.3 Precision metrology and instrumentation

Invar is the traditional material used to make equipment for precision measurement. Due to its extremely low CTE, products such as gauge blocks, interferometer frames, and machine-tool bases not only maintain their calibrated dimensions but also they can be used over different temperatures. Metrology experts emphasize needing ~ 1 ppm dimensional stability in optical mounts; Invar 36 meets this need and has been studied for space-based optical mounts [98].

Invar gauge blocks and scale frames are used as reference standards because their expansion is negligible (NIST notes Invar among materials with small thermal expansion coefficients [99]. For example, telescope mirror mounts often utilize Invar flexures or bezels made of ultra-low-expansion glass (e.g., Zerodur). NASA reports an Invar/Zerodur mirror assembly with support pads that introduced essentially zero distortion (only ~ 5 nm RMS over 28 K) [94].

7.4 Cryogenics and low-temperature systems

The advantages of Invar are also present in the field of cryogenics, where its near zero expansion at cryogenic temperatures makes it a material of choice for cold instruments and storage vessels. The 2021 Invar review emphasizes the application in "cryogenic storage dewars" among others [99]. Actually, the storage vessels for liquid helium and hydrogen are designed with Invar parts in order to reduce the stresses brought about by thermal contraction.

Modern cryogenic optics have also adopted Invar—for example, a 2020 spaceborne infrared spectrometer design used "low-temperature Invar" for its structural framework to withstand a 143 K cooldown (293 → 150 K) without misalignment [100]. This performance has made Invar valuable for precision optical mounts, prism holders, and optical benches tested across large thermal gradients. In the same manner, Invar trusses are the most common support in space cryostats for cold telescope instruments like infrared cameras that require active cooling and therefore cannot be distorted by alignment. Invar 36 is the material of choice for cryocooler components as well as for the focal plane, and this can be seen in NASA's TIRS instrument which is an assembly of Invar parts that work perfectly at ~ 40 K.

7.5 Structural components and tooling

Beyond tooling for aerospace, Invar also finds niche use in specialized structural parts where dimensional stability is critical. Some of the examples are satellite antenna trusses, precision clock components, and refractometer tubes. 3D printed Invar face sheets and stiffeners of a large size are under the stage of testing for the fast production of extremely stable tools and molds in the manufacturing sector [62]. Besides that, there are also copper-clad Invar sheets that deal with expansion in thermal cyclers and laser diode heat spreaders. Invar is also widely used in composite molds for thermoset composites, where it keeps the tool size constant through cure cycles. Its thermal stability makes it ideal for precision frames such as laboratory optical benches and geodetic antenna mounts. More recently, WAAM has enabled the production of lightweight, large-scale Invar components such as fusion targets and cryogenic pumps—that can maintain their shape consistently from room temperature down to cryogenic conditions.

7.6 Medical and emerging applications

While Invar's properties could benefit biomedical instruments, specific recent examples are scarce. Based on the databases and keywords used in this review, very limited peer-reviewed literature was identified on the use of Invar in medical tools during the last decade. It may see limited use in niche areas (e.g., stable optomechanical mounts in surgical microscopes), but documented use is minimal. In contrast, other low-CTE materials (glass–ceramics) dominate high-end medical imaging optics. Nonetheless, precision medical devices requiring micrometer stability could potentially exploit Invar 36 or its variants. As emerging research, the novel Invar-based materials are being developed. Multi-step heat treatments have produced Invar 36 with an ultra-low stable CTE (~ 0.5–0.6 × 10^{-6}/K up to 150 °C) [96], which could open new applications in aerospace and precision electronics. Nonmagnetic Invar-like alloys (e.g. Fe–Ni–Co variants) are also under investigation to combine low expansion with reduced magnetism, benefiting optics and cryogenic instruments.

Invar's uniquely low thermal expansion continues to make it indispensable where dimensional fidelity is critical. In the past 10 years, Invar 36 and its derivatives have been used or studied for space telescopes, semiconductor equipment, precision gauges, and cryogenic instruments. Innovations include composite Cu–Invar substrates for electronics [96], WAAM of Invar for aerospace tooling [62], and advanced thermal processing to further stabilize its dimensions [96]. As high-stability requirements grow (e.g., for exoplanet observatories and nanoscale manufacturing), Invar alloy technology and new alloys inspired by Invar's behavior remain active research areas.

8 Research gaps, challenges, and opportunities

Even though Invar alloys have been studied for a long time, there are still a few important areas of research that have not been fully addressed. These gaps are mainly related to the behavior and performance of Invar alloys when they are produced by additive manufacturing or when they are used in advanced applications.

8.1 Basic mechanisms and thermomagnetic properties of invars

The fact that the Invar effect in Fe–Ni alloys is caused by magneto-volume effects is well established. Still, the connections between magnetic ordering, alloying, and thermal expansion are not completely resolved. There are some studies that give qualitative explanations on this topic, but there are still no quantitative models that can predict how the microstructure, magnetic domain evolution, and CTE will change with temperature. This is a limitation for the design of alloys that have specific thermal responses.

8.2 Additive manufacturing challenges

Although LPBF and DED are additive manufacturing techniques that allow the production of near-net-shape parts, there are some issues that remain:

- Residual stresses and distortion due to rapid heating and cooling cycles
- Porosity and lack of fusion defects that not only affect mechanical properties but also thermal stability
- Anisotropy of microstructure and properties, especially in the build direction

Besides, there is a lack of processing window standards and characterization protocols that would make it easier to verify and compare results by different researchers. Part of the future research should be dedicated to process-structure–property modeling and real-time monitoring to achieve better reproducibility of results.

8.3 Alloy design and compositional engineering

Adding alloying elements (for instance, Co, Cr, WC, TiC) can provide the possibility of increasing strength and keeping the CTE at a low level. However:

- The trade-off between strength and CTE has not been fully exploited
- The roles of trace elements in magnetic transitions and stability over time are hardly known
- Most multi-component and high-entropy Invar-like systems are yet to be discovered

Compositionally engineered alloys in combination with computational tools (e.g., CALPHAD and machine learning) should be the target of future research to provide multifunctional properties in a balanced way.

8.4 Emerging opportunities

Here are some promising options, based on the past and recent research

- Composite or ceramic combined with Invar in multi-material and hybrid structures
- Wear and fatigue resistance by surface engineering
- Nano-structuring for strengthening without thermal stability loss
- AM process control through data-driven optimization and digital twins

In these directions, new breakthroughs can lead to the creation of Invar-based materials, which are more sophisticated and capable of being used in very high precision and harsh environmental conditions.

9 Conclusions

This review served as a detailed and comprehensive up-to-date assessment of Invar alloys and highlighted the integration of these alloys into the AM technologies and the effects on microstructure, mechanical behavior, and thermal stability. The distinctive low CTE of Invar alloy, which results from the magnetic ordering of Fe–Ni, remains the most important property of the material for precision and cryogenic applications. Nevertheless, this review displays that AM methods such as LPBF, DED, WAAM, and CSAM may drastically alter this property due to changes in porosity, texture, residual stress, and local chemical compositions. Throughout the studies referenced, it is clear that with proper optimization of AM parameters, one can produce Invar parts that are closely dense and have CTE values equal to or even lower than those of the conventionally manufactured ones, thus allowing for complex geometries and less material waste. Various post-processing methods, such as heat treatment, stress relief, HIP, and cryogenic treatment, play a critical role in dimensional stability, residual-stress elimination, and mechanical property adjustments while maintaining low thermal expansion. In particular, the right annealing and aging steps can be used to balance the trade-offs between strength, ductility, and magnetic stability, whereas cryogenic treatments assist in improving the tribological properties and the general performance of the material under extremely low temperature applications such as LNG storage, aerospace, and cryogenic space systems. Solid-state methods such as cold spray AM are less likely to lose the ultra-low CTE characteristic by not permitting melting-induced compositional changes and thermal distortion, thus, are more desirable compared to other

AM techniques. Nevertheless, apart from these successes, problems like anisotropy, porosity control, surface finish, and the impact of thermal expansion on minor composition variations, especially nickel evaporation during the high-energy process, still exist. The fixing of these problems will require the enforcement of more stringent process control, the use of both computational and experimental approaches for optimization, and the development of post-processing routes specifically designed for the application. Overall, the integration of AM, advanced thermal treatments, and alloy design makes Invar a very attractive material for next-generation precision tooling, aerospace structures, cryogenic space systems, and high-stability applications that are just emerging, as well as providing concrete directions for future research and industrial implementations.

Acknowledgements Only the authors listed contributed to this article.

Author contributions FA: Original draft, Visualization, Validation; AH: Writing—review and editing, Methodology; GA: Original draft, Formal analysis; AB: Writing—review and editing; RA: Writing—review and editing, Supervision; EA: Writing—review and editing, Supervision, Conceptualization.

Data availability No datasets were generated or analysed during the current study.

Declarations

Conflict of interest The authors declare no conflict of interests.

Open Access This article is licensed under a Creative Commons Attribution 4.0 International License, which permits use, sharing, adaptation, distribution and reproduction in any medium or format, as long as you give appropriate credit to the original author(s) and the source, provide a link to the Creative Commons licence, and indicate if changes were made. The images or other third party material in this article are included in the article's Creative Commons licence, unless indicated otherwise in a credit line to the material. If material is not included in the article's Creative Commons licence and your intended use is not permitted by statutory regulation or exceeds the permitted use, you will need to obtain permission directly from the copyright holder. To view a copy of this licence, visit http://creativecommons.org/licenses/by/4.0/.

References

1. Chen C, Ma B, Liu B, He J, Xue H, Zuo Y, Li X (2019) Refinement mechanism and physical properties of arc melted invar alloy with different modifiers. Mater Chem Phys 227:138–147
2. Liu H, Sun Z, Wang G, Sun X, Li J, Xue F, Peng H, Zhang Y (2016) Effect of aging on microstructures and properties of Mo-alloyed Fe–36Ni invar alloy. Mater Sci Eng A 654:107–112
3. Akgul B, Kul M, Erden F (2024) The puzzling thermal expansion behavior of invar alloys: a review on process-structure-property relationship. Crit Rev Solid State Mater Sci 49(2):254–307
4. Inaba M, Teshima K, Higashinakagawa E, Ohtake Y (2002) Development of an invar (Fe-36Ni) shadow mask for color cathode ray tubes. IEEE Trans Electron Devices 35(10):1721–1729
5. Shiga M (1996) Invar alloys. Curr Opin Solid State Mater Sci 1(3):340–348
6. Oyedeji AN, Sacks N, Venter AM, Marais D, Pötschke J (2025) Optimisation of LPBF process parameters and residual stress analyses of Invar-10wt% TiC and Invar-10wt% TiN metal matrix composites. Prog Addit Manuf 10(8):5117–5133. https://doi.org/10.1007/s40964-024-00892-7
7. Subeshan B, Ali Z, Asmatulu E (2024) Metal additive manufacturing in space and aerospace exploration: current processes, material selection and challenges. J Eng Appl Sci 11(2):35. https://doi.org/10.5455/jeas.2024021104
8. Huang G, He G, Gong X, He Y, Liu Y, Huang K (2024) Additive manufacturing of Invar 36 alloy. J Mater Res Technol 30:1241–1268. https://doi.org/10.1016/j.jmrt.2024.02.221
9. Asgari H, Salarian M, Ma H, Olubamiji A, Vlasea M (2018) On thermal expansion behavior of invar alloy fabricated by modulated laser powder bed fusion. Mater Des 160:895–905. https://doi.org/10.1016/j.matdes.2018.10.025
10. Qiu C, Liu Y, Liu H (2021) Influence of addition of TiAl particles on microstructural and mechanical property development in Invar 36 processed by laser powder bed fusion. Addit Manuf 48:102457. https://doi.org/10.1016/j.addma.2021.102457
11. Bernhard R, Neef P, Hoff C, Hermsdorf J, Kaierle S, Wiche H, Wesling V (2022) Additive manufacturing of optical, thermal and structural components by laser metal deposition. Generative manufacturing of optical, thermal and structural components (GROTESK). Springer, pp 97–117
12. Obidigbo C, Tatman E-P, Gockel J (2019) Processing parameter and transient effects on melt pool geometry in additive manufacturing of Invar 36. Int J Adv Manuf Technol 104(5–8):3139–3146. https://doi.org/10.1007/s00170-019-04229-5
13. Yakout M, Phillips I, Elbestawi MA, Fang Q (2021) In-situ monitoring and detection of spatter agglomeration and delamination during laser-based powder bed fusion of Invar 36. Opt Laser Technol 136:106741
14. Qiu C, Adkins NJE, Attallah MM (2016) Selective laser melting of Invar 36: microstructure and properties. Acta Mater 103:382–395
15. Yang Q, Wei K, Yang X, Xie H, Qu Z, Fang D (2020) Microstructures and unique low thermal expansion of Invar 36 alloy fabricated by selective laser melting. Mater Charact 166:110409
16. Chen C, Xie Y, Liu L, Zhao R, Jin X, Li S, Huang R, Wang J, Liao H, Ren Z (2021) Cold spray additive manufacturing of Invar 36 alloy: microstructure, thermal expansion and mechanical properties. J Mater Sci Technol 72:39–51
17. Ye S, Xu L, Guo Y, Di X, Han Q, Zheng Y, Li X (2025) Microstructure and mechanical properties of super-invar alloy fabricated by wire-arc additive manufacturing. Adv Manuf 2(1):1–20
18. Zhao R, Zhao Y, Qin M, Jia Y, Feng K, Li Z, Ramamurty U, Xie R (2024) Influence of process parameters on properties of Super Invar alloy fabricated by laser powder bed fusion for semiconductor equipment. Addit Manuf 92:104404
19. Zhao R, Shi L, Feng K, Li Z, Xie R (2025) Effect of quenching and tempering on microstructure and properties of Super Invar alloy fabricated by laser powder bed fusion for semiconductor equipment. Prog Addit Manuf 10(12):11891–11917
20. Heine B, Kah A, Sedlmajer M, Ocker C, Merkel M (2022) Impact of corrosion on mechanical properties of additively manufactured Invar 36. Materialwiss Werkst 53(3):316–327
21. Li Y, Guan X, Liu X, Gu H (2025) The effect of TiC addition on the mechanical properties and thermal expansion coefficient during laser metal deposition of invar 36 alloy. Eng Fail Anal 169:109198

22. Mikhailov SB, Sharapova VA, Potekhin BA, Mikhailova NA (2022) Dilatometric effects during annealing of Fe-Ni-C cast Invar alloy. AIP Conf Proc. https://doi.org/10.1063/5.0074768
23. Chavan V, Koch P, Schlüter M, Briese C (2023) Towards realistic evaluation of industrial continual learning scenarios with an emphasis on energy consumption and computational footprint. Proceedings of the IEEE/CVF international conference on computer vision, 11506–11518
24. Qian L (2024) Microwave filters based on advanced manufacture techniques towards high-power applications. University of Birmingham
25. Rao Z, Bajpai A, Zhang H (2024) Active learning strategies for the design of sustainable alloys. Philos Trans A 382(2284):20230242
26. Su Y, Yang X, Wu D, Meng T, Li W, Feng W, Vairis A (2023) Optimizing welding sequence of TIG cross-joint of invar steel using residual stresses and deformations. J Manuf Process 105:232–245
27. Huang G, He G, Liu Y, Huang K (2024) Anisotropy of microstructure, mechanical properties and thermal expansion in invar 36 alloy fabricated via laser powder bed fusion. Addit Manuf 82:104025
28. Liu H, Pan X, Sun P, Liu Y, Qiu C (2024) Influence of addition of Ti particles and processing condition on microstructure and properties of selectively laser-melted Invar 36 alloy. 3D Print Addit Manuf 11(1):24–39. https://doi.org/10.1089/3dp.2022.0016
29. Li XC, Stampfl J, Prinz FB (2000) Mechanical and thermal expansion behavior of laser deposited metal matrix composites of invar and TiC. Mater Sci Eng A 282(1–2):86–90
30. Liu H, Yu Y, Feng L, Wang Y, Sun Z, Zhang J (2024) Promoting nanoprecipitates via prefabricated defects to pin dislocations and grain boundaries for trading off high-strength and low-thermal-expansion of invar alloys. J Alloys Compd 994:174770
31. Mijangos D, Mejia I, Cabrera JM (2022) Influence of microalloying additions (Nb, Ti, Ti/B, V and Mo) on the microstructure of TWIP steels. Metallogr Microstruct Anal 11(3):524–536
32. Zhilin SG, Komarov ON (2023) Promising methods for the formation of bimetallic composite products with high strength in the junction zone of dissimilar materials. Metallurgist 67(7):995–1005
33. Zhao R, Shi L, Liu H, Zhang L, Feng K, Li Z, Xie R (2025) Effect of building-height-dependent heat accumulation on microstructure and properties of Super Invar alloy fabricated by laser powder bed fusion. Mater Charact. https://doi.org/10.1016/j.matchar.2025.115065
34. Zhao W, Wang H, Wang A, Wang L, Liu B, Yang Y, Liu Y (2025) Exploring the origin of the Elinvar effect from lattice distortion in multiple-element alloys. J Mater Sci Technol. https://doi.org/10.1016/j.jmst.2025.09.067
35. Zhao R, Liu H, Feng K, Li Z, Xie R (2025) Effect of solid-solution treatment and cooling method on texture evolution and properties of Super Invar alloy fabricated by laser powder bed fusion. J Alloys Compd. https://doi.org/10.1016/j.jallcom.2025.181191
36. Shen X, Yu X, Lin M, Sun Y, Ding Y, Yan A (n.d.) The influence of quenching temperature on the high-temperature properties and microstructure of fenico alloys
37. Yang S, Yang Q, Qu Z, Wei K (2023) Influence of manufacturing defects on mechanical behavior of the laser powder bed fused invar 36 alloy: in-situ X-ray computed tomography studies. Materials (Basel) 16(8):2956
38. Stephenson T, Tricker D, Tarrant A, Michel R, Clune J (2015) Physical and mechanical properties of LoVAR: a new lightweight particle-reinforced Fe-36Ni alloy. Mater Technol Appl Opt Struct Compon Sub-Syst II 9574:68–74
39. Harrison NJ, Todd I, Mumtaz K (2017) Thermal expansion coefficients in invar processed by selective laser melting. J Mater Sci 52(17):10517–10525. https://doi.org/10.1007/s10853-017-1169-4
40. Huang L, Zhou Y, Guo T, Han D, Gu Y, Song C, Pan F (2022) Investigation of temperature-dependent magnetic properties and coefficient of thermal expansion in Invar alloys. Materials 15(4):1504. https://doi.org/10.3390/ma15041504
41. Hitzler L, Shahul Hameed MZ, Kah A, Merkel M, Werner E (2022) Thermal expansion and temperature-dependent Young's modulus of Invar fabricated via laser powder-bed fusion. Prog Addit Manuf 7(3):463–470. https://doi.org/10.1007/s40964-022-00299-2
42. Liu X, Yu Y, Zhang S, Li J, Liu H, Zhang J, Sun Z, Yan W (2025) Deformation mechanism and properties evolution of V<sc>–</sc>N invar alloy with high strength after cold rolling and subsequent aging treatment. Mater Charact 228(June):115383. https://doi.org/10.1016/j.matchar.2025.115383
43. Zhang S, Liu X, Liu H, Yu Y, Chang C, Di Y (2025) Microstructure evolution and strengthening mechanism of VN microalloyed Invar alloy processed by mechanical heat treatment. Materials 18(17):3934
44. Yusupova NR, Krylova KA, Mulyukov RR (2023) Effect of microstructure on the strength of nanostructured Invar 36 alloy. Lett Mater 13(3):255–259. https://doi.org/10.22226/2410-3535-2023-3-255-259
45. Fan W, Zhang C, Tan H, Wang Y, Peng Y, Zhang F, Lin X, Huang W (2022) Microstructures and mechanical properties of Invar/MnCu functionally graded material fabricated by directed energy deposition. Mater Sci Eng A 860:144332
46. Hidalgo J, Jiménez-Morales A, Barriere T, Gelin JC, Torralba JM (2014) Mechanical and functional properties of Invar alloy for μ-MIM. Powder Metall 57(2):127–136
47. Nagayama T, Yamamoto T, Nakamura T (2016) Thermal expansions and mechanical properties of electrodeposited Fe–Ni alloys in the Invar composition range. Electrochim Acta 205:178–187
48. Ren G, Cui Z, Hao X, Qiu D, Zhang H, Wang W, Li W (2024) Effect of subgrain microstructure on the mechanical properties of Invar 36 specimens prepared by laser powder bed fusion. J Alloys Compd 1004:175839
49. Wei K, Yang Q, Ling B, Yang X, Xie H, Qu Z, Fang D (2020) Mechanical properties of Invar 36 alloy additively manufactured by selective laser melting. Mater Sci Eng A 772:138799. https://doi.org/10.1016/j.msea.2019.138799
50. Meboldt M, Klahn C (2018) Industrializing additive manufacturing: proceedings of additive manufacturing in products and applications: AMPA2017. Springer
51. Inagaki ITTYS, Ariyasu N (2014) Application and features of titanium for the aerospace industry. Nippon Steel Sumitomo Metal Tech Rep 106(106):22–27
52. Lores A, Azurmendi N, Agote I, Espinosa E, García-Blanco MB (2022) A study of parameter and post-processing effects on surface quality improvement of binder jet 3D-printed Invar36 alloy parts. Prog Addit Manuf 7(5):917–930. https://doi.org/10.1007/s40964-022-00267-w
53. Subeshan B, Baddam Y, Asmatulu E (2021) Current progress of 4D-printing technology. Prog Addit Manuf 6(3):495–516. https://doi.org/10.1007/s40964-021-00182-6
54. Singh R, Gupta A, Tripathi O, Srivastava S, Singh B, Awasthi A, Rajput SK, Sonia P, Singhal P, Saxena KK (2020) Powder bed fusion process in additive manufacturing: an overview. Mater Today Proc 26:3058–3070. https://doi.org/10.1016/j.matpr.2020.02.635
55. Dejene ND, Lemu HG (2023) Current status and challenges of powder bed fusion-based metal additive manufacturing: literature review. Metals 13(2):424. https://doi.org/10.3390/met13020424
56. Uhlmann E, Kersting R, Klein TB, Cruz MF, Borille AV (2015) Additive manufacturing of titanium alloy for aircraft components. Procedia CIRP 35:55–60. https://doi.org/10.1016/j.procir.2015.08.061

57. Nuñez L, Downey CM, van Rooyen IJ, Charit I, Maughan MR (2024) Analysis of surface roughness in metal directed energy deposition. Int J Adv Manuf Technol. https://doi.org/10.1007/s00170-024-13587-8
58. Feilden E (2017) Additive manufacturing of ceramics and ceramic composites via robocasting. Imperial College London
59. Lin F, Wan J, Yang D, Ke Y, Yang H, Lin X, Chen Y (2026) Achieving high strength and low thermal expansion coefficient in additively manufactured invar alloys by leveraging the effect of alloying elements. J Mater Sci Technol 254:81–93. https://doi.org/10.1016/j.jmst.2025.08.006
60. Wegener T, Brenne F, Fischer A, Möller T, Hauck C, Auernhammer S, Niendorf T (2021) On the structural integrity of Fe-36Ni invar alloy processed by selective laser melting. Addit Manuf 37:101603. https://doi.org/10.1016/j.addma.2020.101603
61. Yang Q, Wei K, Qu Z, Yang X, Fang D (2024) In-situ X-ray computed tomography of high-temperature tensile behavior for laser powder bed fused invar 36 alloy. Addit Manuf 83:104072. https://doi.org/10.1016/j.addma.2024.104072
62. Veiga F, Suarez A, Aldalur E, Artaza T (2022) Wire arc additive manufacturing of invar parts: bead geometry and melt pool monitoring. Measurement 189:110452. https://doi.org/10.1016/j.measurement.2021.110452
63. Jiao G, Fang X, Chen X, Xi N, Zhang M, Liu Y, Wu H, Huang K (2023) The origin of low thermal expansion coefficient and enhanced tensile properties of Invar alloy fabricated by directed energy deposition. J Mater Process Technol 317:117994. https://doi.org/10.1016/j.jmatprotec.2023.117994
64. Bobbio LD, Otis RA, Borgonia JP, Dillon RP, Shapiro AA, Liu Z-K, Beese AM (2017) Additive manufacturing of a functionally graded material from Ti-6Al-4V to Invar: experimental characterization and thermodynamic calculations. Acta Mater 127:133–142. https://doi.org/10.1016/j.actamat.2016.12.070
65. Aldalur E, Suárez A, Veiga F (2022) Thermal expansion behaviour of Invar 36 alloy parts fabricated by wire-arc additive manufacturing. J Mater Res Technol 19:3634–3645. https://doi.org/10.1016/j.jmrt.2022.06.114
66. Chen C, Zhao C, Sun Z, He J, Guo W, Xue H, Liu B, Zhang C, Zhang H (2025) Microstructure characteristics and mechanical properties of high-strength Invar alloy by wire arc additive manufacturing. Appl Sci (Basel) 15(6):3351. https://doi.org/10.3390/app15063351
67. Mattera G, Manoli E, Nele L (2025) Study on the printing stability of Invar 36 alloy under different process parameter conditions in gas metal arc additive manufacturing. Mater Sci Addit Manuf 4(4):025220046. https://doi.org/10.36922/MSAM025220046
68. Gil Del Val A, Cearsolo X, Suarez A, Veiga F, Altuna I, Ortiz M (2023) Machinability characterization in end milling of Invar 36 fabricated by wire arc additive manufacturing. J Mater Res Technol 23:300–315. https://doi.org/10.1016/j.jmrt.2022.12.182
69. Yin J, Zhang W, Ke L, Wei H, Wang D, Yang L, Zhu H, Dong P, Wang G, Zeng X (2021) Vaporization of alloying elements and explosion behavior during laser powder bed fusion of Cu–10Zn alloy. Int J Mach Tools Manuf 161:103686. https://doi.org/10.1016/j.ijmachtools.2020.103686
70. Williams SW, Martina F, Addison AC, Ding J, Pardal G, Colegrove P (2016) Wire + arc additive manufacturing. Mater Sci Technol 32(7):641–647. https://doi.org/10.1179/1743284715Y.0000000073
71. Yin S, Cavaliere P, Aldwell B, Jenkins R, Liao H, Li W, Lupoi R (2018) Cold spray additive manufacturing and repair: fundamentals and applications. Addit Manuf 21:628–650. https://doi.org/10.1016/j.addma.2018.04.017
72. Yakout M, Elbestawi MA, Veldhuis SC, Nangle-Smith S (2020) Influence of thermal properties on residual stresses in SLM of aerospace alloys. Rapid Prototyp J 26(1):213–222. https://doi.org/10.1108/RPJ-03-2019-0065
73. DebRoy T, Wei HL, Zuback JS, Mukherjee T, Elmer JW, Milewski JO, Beese AM, Wilson-Heid A, De A, Zhang W (2018) Additive manufacturing of metallic components: process, structure and properties. Prog Mater Sci 92:112–224. https://doi.org/10.1016/j.pmatsci.2017.10.001
74. Mushnikov NV, Popov AG, Gaviko VS, Protasov AV, Kleinerman NM, Golovnya OA, Naumov SP (2022) Peculiarities of phase diagram of Fe-Ni system at Ni concentrations 0–20 at.%. Acta Mater 240:118330. https://doi.org/10.1016/j.actamat.2022.118330
75. Gutfleisch O, Willard MA, Brück E, Chen CH, Sankar SG, Liu JP (2011) Magnetic materials and devices for the 21st century: stronger, lighter, and more energy efficient. Adv Mater 23(7):821–842. https://doi.org/10.1002/adma.201002180
76. Wang B, Guo Y, Zhang Z, Yi X, Wang D (2023) Investigation of cryogenic friction and wear properties of Invar 36 alloy against Si3N4 ceramic balls. Wear 518–519:204648. https://doi.org/10.1016/j.wear.2023.204648
77. Kul M, Akgül B, Karabay YZ, Hitzler L, Sert E, Merkel M (2024) Minimum and stable coefficient of thermal expansion by three-step heat treatment of Invar 36. Crystals 14(12):1097. https://doi.org/10.3390/cryst14121097
78. Van Swygenhoven H, Derlet PM, Hasnaoui A (2002) Atomic mechanism for dislocation emission from nanosized grain boundaries. Phys Rev B 66(2):024101. https://doi.org/10.1103/PhysRevB.66.024101
79. Li B, Shen X, Zhou D, Huang M, Zhou B, Liu L, Sun Y, Ding Y, Yan A (2025) Combination strategy for high-performance Invar 36 soft magnetic alloy: synergistic improvement of the heat treatment process. J Alloys Compd 1017:179171. https://doi.org/10.1016/j.jallcom.2025.179171
80. Takenaka K (2012) Negative thermal expansion materials: technological key for control of thermal expansion. Sci Technol Adv Mater 13(1):013001. https://doi.org/10.1088/1468-6996/13/1/013001
81. Park SJ, Jo S-H, Kim JG, Kim J, Lee R, Oh Y-S, Kim S-J, Lee HW, Kang S-H, Jung J (2022) Evolution of microstructure, mechanical properties and residual stress of a cold rolled invar sheet due to heat treatment. Metals 12(1):110. https://doi.org/10.3390/met12010110
82. Nishiyama S, Honda Y, Sato D, Tanabe H (1995) Effects of cold rolling and annealing conditions on recrystallization and r-value in invar alloy. Tetsu to Hagane 81(11):1097–1102. https://doi.org/10.2355/tetsutohagane1955.81.11_1097
83. Çakır A (2019) Effect of Al doping on the magnetic and elastic properties of Fe65Ni35 invar alloys. Turk J Phys 43(1):109–115
84. Heine B, Kah A, Sedlmajer M, Ocker C, Merkel M (2022) Impact of corrosion on mechanical properties of additively manufactured Invar 36. Materialwiss Werkstofftech 53(3):316–327
85. Wei C, Gu H, Li Q, Sun Z, Chueh Y, Liu Z, Li L (2021) Understanding of process and material behaviours in additive manufacturing of Invar36/Cu10Sn multiple material components via laser-based powder bed fusion. Addit Manuf 37:101683. https://doi.org/10.1016/j.addma.2020.101683
86. He G, Peng X, Zhou H, Huang G, Xie Y, He Y, Liu H, Huang K (2023) Superior mechanical properties of Invar36 alloy lattices structures manufactured by laser powder bed fusion. Materials 16(12):4433. https://doi.org/10.3390/ma16124433
87. Li H, Chen B, Tan C, Song X, Feng J (2020) Microstructure evolution and mechanical properties of laser metal deposition of Invar 36 alloy. Opt Laser Technol 125:106037
88. Tan H, Wang Y, Wang G, Zhang F, Fan W, Feng Z, Lin X (2020) Investigation on microstructure and properties of laser solid formed low expansion Invar 36 alloy. J Mater Res Technol 9(3):5827–5839. https://doi.org/10.1016/j.jmrt.2020.03.108

89. Oh DJ, Lee JM, Kim MH (2014) Fatigue assessment of thin welded joints from invar alloy by local stress concept. Mater Technol Pet Technol. https://doi.org/10.1115/OMAE2014-23825
90. Choi S, Won J, Lee J-J, Lee H-K, Kim S-M, Cho C, Kwon D (2020) Evaluation of cryogenic mechanical properties of resistance seam-welded Invar alloy sheet by instrumented indentation test. J Mar Sci Eng 8(12):1009
91. Ona K, Sakaguchi N, Ohno H, Utsunomiya S (2020) The advanced super Invar alloys with zero thermal expansion for space telescopes. Trans Japan Soc Aeronaut Space Sci Aerosp Technol Japan 18(3):32–37. https://doi.org/10.2322/tastj.18.32
92. Dsouza LA, Mendonca V (2025) Comparative analysis of surface roughness and tool wear under dry, MQL, and cryogenic machining conditions in invar 36 turning operations. J Mines Metals Fuels 73(4):1097–1105. https://doi.org/10.18311/jmmf/2025/47546
93. Cleveland P, Glazer S, Packard E (2010) Enhancements to the NASA/goddard space flight center (GSFC) space environment simulator (SES) facility to support cryogenic testing of the james webb space telescope (JWST) integrated science instrument module (ISIM). 40th International conference on environmental systems. https://doi.org/10.2514/6.2010-6167
94. NASA Science Editorial Team (2025) A new alloy is enabling ultra-stable structures needed for exoplanet discovery
95. Veiga F, Suárez A, Artaza T, Aldalur E (2022) Effect of the heat input on wire-arc additive manufacturing of Invar 36 alloy: microstructure and mechanical properties. Weld World 66(6):1081–1091. https://doi.org/10.1007/s40194-022-01295-4
96. Nie Q, Chen G, Wang B, Yang L, Zhang J, Tang W (2022) Effect of Invar particle size on microstructures and properties of the Cu/Invar bi-metal matrix composites fabricated by SPS. J Alloys Compd 891:162055. https://doi.org/10.1016/j.jallcom.2021.162055
97. Hertzberg HT (1987) Invar foil. European Patent Application, Germany
98. Thakar RA, Trivedi SV (2017) An overview of dimensional stability of invar 36 material for space based optical mounting applications. Int Conf Ideas Impact Innov Mech Eng 5(6):146–151
99. Sahoo A, Medicherla VRR (2021) Fe-Ni Invar alloys: a review. Mater Today Proc 43:2242–2244. https://doi.org/10.1016/j.matpr.2020.12.527
100. Li C, Ding Y, Lin C, Wei Y, Zheng Y, Zhang L (2020) Optomechanical design and simulation of a cryogenic infrared spectrometer. Appl Opt 59(15):4642. https://doi.org/10.1364/AO.392621

Publisher's Note Springer Nature remains neutral with regard to jurisdictional claims in published maps and institutional affiliations.